Identification of an antiretroviral small molecule that appears to be a host-targeting inhibitor of HIV-1 assembly

Jonathan C. Reed[a], Dennis Solas[b], Anatoly Kitaygorodskyy[b], Beverly Freeman[b], Dylan T. B. Ressler[a], Daryl J. Phuong[a], J. Victor Swain[a], Vishwanath R. Lingappa[b], and Jaisri R. Lingappa[a]#

[a]Dept. of Global Health, University of Washington, Seattle, WA. 98109

[b]Prosetta Biosciences, San Francisco, CA 94107

Running Head: Host-targeting inhibitor of HIV-1 assembly

#Address correspondence to Jaisri R. Lingappa, jais@uw.edu.

Abstract

There is an urgent need for development of antiretrovirals that act by novel mechanisms allowing treatment of multidrug resistant HIV-1. Host-targeting drugs are of special interest because they can offer a high barrier to resistance. Here we report identification of potent antiretroviral small molecules that inhibit viral late events, a stage of the HIV-1 life cycle for which potent and specific inhibitors are lacking. These drugs were discovered using cell-free protein synthesis and assembly systems that recapitulate intracellular host-catalyzed viral capsid assembly pathways. The drugs inhibit HIV-1 replication in human T cell lines and PBMCs with nanomolar EC50 values, and are effective against an HIV-1 primary isolate. Drug treatment dramatically reduces virus production, and appears to inhibit a post-translation step HIV-1 Gag assembly. Notably, the drugs colocalize with HIV-1 Gag *in situ*. However, unexpectedly, drug selection failed to identify drug-specific resistance mutations in Gag or any other viral gene product, despite development of resistance mutations in a parallel Nelfinavir selection control. Thus, we hypothesized that instead of binding to Gag directly, this drug might localize to assembly intermediates, the intracellular multiprotein complexes containing Gag and host factors that are formed during immature HIV-1 capsid assembly. Indeed, imaging of infected cells showed colocalization of the drug with ABCE1 and DDX6, two host enzymes found in assembly intermediates. While the exact target and mechanism of action of the drugs remain to be determined, these findings suggest that they may represent first-in-class, host-targeting inhibitors of intracellular events in HIV-1 assembly.

51 **Introduction**

52 In an era in which HIV-1 vaccine trial results have been disappointing, antiretroviral (ARV) drugs
53 stand out as a stunning success story, both for treatment and prevention of HIV-1 infection. Treatment
54 with combined antiretroviral therapy (ART) over the past three decades has resulted in enormous
55 reductions in morbidity and mortality from HIV-1 infection, with 62% of the 38 million people living
56 with HIV receiving antiretroviral drugs in 2018 (1). ART is also the mainstay of PREP, a remarkably
57 successful approach to preventing HIV-1 infection (1, 2). Additionally, ART will be important for
58 future HIV cure strategies. Unfortunately, the success of HIV ART is at risk of being undermined by
59 the increasingly serious problem of HIV-1 drug resistance (3). Virologic failure is seen in up to 20% of
60 individuals receiving first-line ART in low and middle-income countries (4), with up to half of first-line
61 ART failures in sub-Saharan Africa involving resistance to all three drugs in Tenofivir-containing
62 regimens (5). Moreover, the prevalence of drug-resistant HIV-1 is predicted to increase substantially
63 over time as more people receive treatment (6). Indeed, experts have drawn analogies between the
64 future of ART and the current crisis of multidrug resistant tuberculosis (7). For this reason, identifying
65 novel targets in the HIV-1 life cycle and candidate small molecules that inhibit these targets is of high
66 priority, with the goal of driving development of new ARV drugs.

67 Identification of new druggable targets in the poorly understood stages of the viral life cycle will be
68 particularly important for development of drugs aimed at HIV-1 strains resistant to currently available
69 drugs. Mapping the targets of drugs currently in use onto the HIV-1 life cycle reveals a striking lack of
70 drugs that target intracellular events of assembly (8). Currently available ARV drugs target steps in the
71 entry and post-entry stages of the viral life cycle as well as maturation, the final step required to form an
72 infectious virus. In contrast, no approved ARV drugs target intracellular viral late events (Fig 1A),
73 which include post-translational events of immature capsid assembly. Formation of a single infectious
74 virus requires assembly of ~3000 copies of the HIV-1 Gag protein, which are synthesized and
75 oligomerize in the cytoplasm and subsequently target to the plasma membrane, where they encapsidate

76 the HIV-1 genome while multimerizing to form the immature capsid. The immature capsid then
77 undergoes envelopment, budding, release, and maturation (Fig 1A). Interest in targeting HIV-1
78 assembly has been high, leading to numerous drug screens in recent years (9, 10). Of the compounds
79 identified in these screens, the most successful have been those that bind to the capsid protein (CA). CA
80 is critical at multiple stages of the viral life cycle including immature capsid assembly, maturation,
81 infectivity, and post-entry events (Fig 1A). Interestingly, potent small molecules that target CA do not
82 selectively inhibit immature capsid assembly (reviewed in (9)– instead they either act preferentially on
83 the mature capsid, targeting virion infectivity and post-entry events (e.g. PF74 (11-15)), or act broadly
84 on Gag synthesis, assembly, and post-entry events (e.g. GS-CA1, (16)). Indeed, to our knowledge, there
85 are no reports of a potent small molecule identified in any screen that selectively inhibits intracellular
86 HIV-1 late events.

87 We hypothesized that one reason for the failure to identify selective inhibitors of HIV-1 assembly
88 might be that previous screens were either very broad or very narrow – i.e. they encompassed the entire
89 viral life cycle (e.g.(17)) and therefore selected for the most easily inhibited stages of the life cycle, or
90 they were based solely on multimerization of recombinant CA-derived peptides *in vitro* and therefore
91 lacked other critical interfaces (e.g.(18)). We further hypothesized that a screen that focuses on post-
92 translational events of Gag assembly and includes known cellular facilitators of immature HIV-1 capsid
93 assembly could be more successful than other screens in identifying a selective inhibitor of intracellular
94 events in HIV-1 assembly. Specifically, while recombinant Gag is able to assemble into immature
95 capsid-like particles in the absence of host proteins (reviewed in (19)), two decades of studies support a
96 different model for HIV-1 assembly in cells – one in which Gag assembles into immature capsids via a
97 pathway of assembly intermediates containing viral proteins, as well as host proteins that act
98 catalytically to promote HIV-1 capsid assembly (e.g.(20-30); Fig 1B). This model suggests that to
99 succeed in the hostile environment of the cytoplasm, Gag may have evolved to utilize host proteins to
100 catalyze Gag multimerization, promote RNA packaging, and sequester assembly within host complexes

101 where nascent virions would be less vulnerable to host defenses. If this host-catalyzed model of capsid
102 assembly in the cytoplasm is valid, a screen that recapitulates this host-catalyzed assembly pathway
103 might succeed in identifying novel antiviral compounds.

104 Indeed, a precedent exists for the success of such screens that recapitulate host-catalyzed assembly
105 pathways. Previously our group in collaboration with the CDC used a cell-extract-based screen that
106 recapitulated an intracellular assembly pathway for rabies virus to identify the first reported small
107 molecule inhibitor of rabies replication in cell culture (31). Notably, this small molecule binds to a
108 multiprotein complex that contains ABCE1, a host enzyme identified in HIV-1 assembly intermediates
109 as noted above, suggesting that similar host complexes may be involved in the assembly of diverse
110 viruses.

111 Motivated by the rabies virus precedent and the failure of selective HIV-1 assembly inhibitors to be
112 identified to date, we developed cell-extract-based assembly pathway screens and used them to identify
113 a novel and potent antiretroviral small molecule inhibitor of HIV-1replication, PAV117, and its analog
114 PAV206. Here we present evidence suggesting that PAV117 inhibits HIV-1 replication by interfering
115 with HIV-1 assembly. We found that a tagged analog of these compounds colocalizes with Gag *in situ*.
116 However, notably, non-synonymous mutations did not arise in Gag or Pol after 37 weeks of selection in
117 HIV-1-infected human cells, in stark contrast to Nelfinavir selection examined in parallel, suggesting a
118 high barrier for resistance to this compound. Additional imaging studies shed more light on this
119 apparent barrier to development of viral protein mutations by demonstrating that PAV117 also
120 colocalizes with two host proteins found in HIV-1 capsid assembly intermediates, the enzymes ABCE1
121 and DDX6. While the exact target and mechanism of action of PAV117/PAV206 remain unclear, these
122 studies raise the possibility that these compounds represent a class of novel host-targeting ARV small
123 molecules that inhibits HIV-1 virus production by acting on host-protein-containing capsid assembly
124 intermediates.
125

126 **Results**

127 **Development of a novel screen for capsid assembly inhibitors based on the host catalyzed assembly**
128 **pathway**

129 The first evidence that immature HIV-1 capsids assemble via a host-catalyzed pathway of
130 intermediates was generated in a cell-free system. Adapted from the *in vitro* translation systems that
131 were used to identify signal sequences (32), this cell-free assembly system supports *de novo* synthesis of
132 HIV-1 Gag from a Gag mRNA using energy substrates, amino acids, and a cellular extract that provides
133 host factors required for Gag translation as well as post-translational events of Gag assembly. When
134 programmed with wild-type Gag mRNA, this system produces particles that closely resemble completed
135 immature HIV-1 capsids produced by HIV-1 produced by provirus-expressing cells in their
136 ultrastructural details as well as in their size and shape (as defined by a sedimentation value of ~750S;
137 (24)). Pulse-chase studies of this cell-free assembly system revealed sequential progression of Gag
138 through complexes of increasing size (~10S to ~80S/150S to ~500S to ~750S), consistent with these
139 smaller complexes being intermediates in the formation of the ~750S completely assembled immature
140 capsid. Moreover, Gag mutants that had been defined by others to be assembly-defective in cells are
141 arrested at specific steps of the cell-free assembly pathway, with assembly-competent Gag mutants
142 progressing through the entire pathway (24, 33). Notably, biochemical analysis demonstrated that post-
143 translational events in this assembly pathway required ATP, indicating that HIV-1 immature capsid
144 assembly in cells is energy-dependent (24).

145 In the past two decades, the HIV-1 capsid assembly pathway has been largely studied in cellular
146 systems. Key features of the assembly pathway were identified in cells expressing the HIV-1 provirus
147 (reviewed in (28)), including the sequential progression of Gag through the pathway of assembly
148 intermediates (22), the energy dependence (21), and the arrest of known assembly-defective Gag
149 mutants at specific steps in the pathway (21-24, 28, 29, 34). The energy dependence of this assembly
150 pathway was subsequently explained by the finding that the assembly intermediates contain two host

151 enzymes that facilitate assembly - the ATPase ABCE1 and the Dead Box RNA helicase DDX6 (26, 30).
152 Other studies suggest that packaging of the HIV-1 genome appears to occur in the assembly
153 intermediates (20), and that other lentiviruses utilize analogous assembly pathways (21, 27).
154 Immunoprecipitation and imaging studies confirmed the association of ABCE1 and DDX6 with
155 assembling Gag and identified two other enzymes in assembly intermediates, AGO2 and DCP2 (20, 22,
156 23, 26-29). The finding that assembly intermediates contain at least three proteins typically found in
157 host RNA granules, DDX6, AGO2, and DCP2, supports a model in which assembling Gag co-opts a
158 unique subclass of host RNA granules during assembly. RNA granules are involved in all aspects of
159 host RNA metabolism except translation, and therefore could allow assembling capsids to be
160 sequestered from the innate immune system while at the same time accessing the viral genome, which
161 behaves like a host mRNA, and accessing enzymes that likely facilitate packaging and assembly (Fig
162 1B).
163 While the cellular studies described above demonstrated the physiological relevance of the HIV-1
164 assembly pathway, the cell-free system in which it was identified holds great promise as a drug screen.
165 A cell-free assembly drug screen would have the advantage of recapitulating evolutionarily conserved
166 viral-host interactions critical for assembly while being much less expensive than drug screens that
167 utilize infected cell lines in culture. Additionally, the cell-free system can be adapted for a moderately
168 high-throughput format. Together, these features of a cell-free assembly pathway drug screen allow a
169 large number of compounds to be screened in a cost-effective manner.
170 For these reasons, we adapted the HIV-1 cell-free assembly reaction to generate a drug screen (Fig
171 1C). Cell free reactions, upon completion, contain assembly intermediates and fully assembled
172 immature capsid-like particles, unless performed in the presence of an inhibitor of assembly, in which
173 case Gag will be largely unassembled (i.e. monomers and dimers). Plate-bound anti-Gag antibodies
174 capture monomeric, dimeric, and multimerized Gag from the reaction. To determine how much Gag
175 multimerization occurred during the reaction, a soluble anti-Gag detection antibody is added. The

176 detection antibody does not bind Gag monomers (since the monomer antigenic site is already bound by
177 capture antibody) but would be expected to bind to unoccupied Gag proteins in multimers. Signal from
178 bound detection antibody is quantified using a fluorescent detection system, with more signal being
179 generated by Gag multimers. Thus, an effective inhibitor of Gag multimerization will be recognized by
180 reduction in detection antibody signal (Fig 1C). Because we are interested in inhibitors of assembly
181 rather than protein synthesis, we utilized a counter screen to detect all small molecules that inhibit
182 translation of GFP in cell-free reactions. Compounds that inhibited GFP translation were eliminated
183 from consideration.
184

185 **Identification of a potent inhibitor of HIV-1 replication**

186 Once this cell-free HIV-1 assembly screen and counter screen were successfully established and
187 validated, similar cell-free screens were established for quantifying assembly of the capsids of seven
188 other viruses (Fig 1D). A compound library of ~150,000 small molecules with drug-like characteristics
189 was screened against these eight cell-free assembly assays, resulting in a master hit collection of 249
190 small molecules that inhibited assembly in one or more virus assembly screen(s), but did not
191 significantly inhibit GFP translation.

192 Compounds in the master hit collection were further screened for their ability to inhibit replication of
193 HIV-1 in the MT2 human T cell line. The compound with the most favorable characteristics in this
194 assay was PAV117, a tetrahydroisoquinolone derivative with excellent drug-like properties (Fig 2A).
195 PAV117 inhibits replication of HIV-1 NL4-3 in MT-2 cells with a 50% reduction in virus replication at
196 48 nM (EC50) and a 50% reduction in cell viability at 1.1 mM (CC50; Fig 2B). The nanomolar EC50
197 and a selectivity index (CC50/EC50) of 23 make PAV117 an excellent compound for further
198 optimization. Notably, PAV117 was not active against influenza virus (Fig 2C) or feline
199 immunodeficiency virus, a non-primate lentivirus that is related to HIV-1 (Fig 2D), suggesting that it is

200 not a broadly acting antiviral but instead acts with some specificity on a subset of viruses. Additionally,
201 we found that PAV117 was active against a primary isolate of HIV-1 (Fig 2E).
202
203 **Defining the step in the viral life cycle at which the novel small molecule acts**
204 To determine whether PAV117 acts on entry or post-entry events in the HIV-1 life cycle, MT-2 cells
205 were infected in the presence of PAV117 or DMSO with a luciferase-encoding HIV-1 reporter virus that
206 undergoes only one round of replication (Fig 3A, diagram). PAV117 did not reduce luciferase activity
207 in this assay at non-toxic concentrations (Fig 3A, graph; EC50 of 0.93 mM » CC50 of 1.1 mM),
208 indicating that it does not act early in the HIV-1 life cycle. The effect of PAV117 on viral late events
209 (events that occur after integration) was assayed using chronically infected H9 T cells, which produce
210 infectious virus from integrated HIV-1 provirus (Fig 3B, diagram). In this assay, PAV117 inhibited
211 production of infectious virus, with an EC50 of 104 nM (Fig 3B, black dose-response curve in graph).
212 Thus, all of the activity of PAV117 can be attributed to inhibition of viral late events. To determine
213 whether PAV117 results in production of non-infectious virus, we quantified production of p24 Gag in
214 virus-like particles (VLPs) pelleted from cell culture supernatants of chronically infected H9 cells
215 treated with PAV117 or DMSO. If PAV117 reduced infectivity but not p24 Gag in virus pellets, that
216 would indicate production of non-infectious virus particles. However, we found that inhibition of p24
217 production (Fig 3B, blot) was similar to inhibition of supernatant infectivity (EC50 of 113 nM vs. 104
218 nM, respectively; compare blue vs. black curve in Fig 3B). Western blots of virus-like particles in
219 supernatants also showed no change in the ratio of p55 to p24 with increasing PAV117 concentration
220 relative to DMSO treatment (Fig 3B, blot), indicating that it does not inhibit Gag cleavage required for
221 virus maturation. Thus, the entire effect of PAV117 is due to inhibition of virus production at an
222 intracellular step during the viral late events.
223 The finding that PAV117 does not inhibit Gag cleavage, which occurs during and after budding of
224 immature virus from cells, but does inhibit virus production indicated that PAV117 likely acts on an

225 intracellular late event that precedes maturation. Intracellular events required for virus particle
226 production include transcription of the full-length HIV-1 mRNA, translation of this mRNA to produce
227 Gag and GagPol, assembly of Gag to produce immature capsids, and budding at the plasma membrane
228 to release immature virus. We hypothesized that PAV117 likely acts on post-translational events in
229 assembly of immature HIV-1 capsids for two reasons: first, because a counterscreen was utilized to
230 eliminate inhibitors of translation; and second, because the cell-free screens that identified PAV117
231 recapitulate capsid protein assembly but not virus budding and release. To test this hypothesis, we
232 analyzed acutely infected MT-2 cells treated with DMSO or PAV117 at 0.25 nM vs. 0.75 nM (~EC70
233 and ~EC90). As expected, we observed a dramatic, dose-dependent reduction in p24 release into the
234 supernatant (Fig 4A). Consistent with PAV117 not being an inhibitor of translation, steady-state levels
235 of actin and GAPDH were minimally affected (Fig 4B). At the highest PAV117 concentration tested,
236 some reduction in steady-state Gag levels was observed (Fig 4A), but it was much less than the
237 reduction in VLP production raising the possibility that it is due to degradation of Gag-containing
238 complexes that are bound to PAV117. To further define where PAV117 acts, we also examined steady
239 state levels of HIV-1 capsid assembly intermediates, whose distinct S values allow them to be separated
240 by velocity sedimentation. PAV117 had little to no effect on levels of the ~10S and ~80S/150S
241 intermediates, as % of total Gag (Fig 4C). However, PAV117 resulted in a dose-dependent decrease in
242 the steady-state level of the ~500S intermediate. While these data provide a snapshot of Gag levels at
243 only one point in time, taken together with the dramatic reduction in VLP production, they suggest that
244 PAV117 acts during virus assembly, most likely inhibiting formation of the ~500S assembly
245 intermediate.
246
247 **Generation of analogs of the novel small molecule inhibitor that are more potent and tagged**
248 If PAV117 acts during assembly, one might expect it to be associated with assembling HIV-1 Gag.
249 To test if this is the case, we needed an analog of PAV117 that contains a tag, such as biotin, to allow

250 detection while retaining its antiviral activity. To identify positions that could be used for a biotin tag,
251 structure-activity relationships were analyzed with various combinations of methyl, methoxy, or
252 benzoyloxy substitutions in the R1, R2, and R3 positions of the pendant benzene ring (Fig 5A).
253 Interestingly, we observed that the presence of a methyl in the R1 position and a and a methoxy in the
254 R2 position (PAV218 and PAV206) resulted in reduced toxicity (higher CC50) and a higher selectivity
255 index when analyzed in HIV-1 infected MT-2 T cells (Fig 5A). PAV206 was particularly notable since
256 it had a lower EC50 and much higher CC50 than PAV117, resulting in an excellent SI of 62-82 in MT-2
257 cells (Fig 5A, B) and ~48 in HIV-1 infected PBMCs (Fig 5B).
258 The structure-activity relationship analysis also led to identification of a strategy for introducing a
259 biotin tag into PAV206 (or PAV117), by revealing that the R3 position on the dependent benzene ring is
260 not critical for activity. Specifically, this position can tolerate either a bulky group (as in PAV117) or a
261 hydrogen (as in PAV218) without loss of activity (Fig 5A). For this reason, a biotin was introduced at
262 this position, generating the PAV818 analog (Fig 5C). PAV818 is identical to PAV117 and PAV206
263 except at the R3 position, which is a biotin in PAV818. PAV818 has a higher EC50 (951 nM) than the
264 PAV117 or PAV206 analogs, but also had a remarkably high CC50 (~30 mM), giving it a respectable SI
265 of ~32 (Fig 5C). Thus, PAV818 represents a biotinylated analog of PAV117 and PAV206 that can be
266 utilized to visualize where these compounds localize within infected cells.
267
268 **A tagged analog of PAV117 colocalizes with HIV-1 Gag *in situ* in infected cells**
269 Next we utilized the biotinylated antiviral analog PAV818 to ask if this family of compounds
270 colocalizes with HIV-1 Gag as one would expect if they inhibit assembly, as suggested by data in Fig 4.
271 For this purpose, we used the proximity ligation assay (PLA), a technique which marks two proteins that
272 are in close proximity with fluorescent spots. Briefly, in PLA, primary antibodies from two species are
273 detected by species-specific secondary antibodies that are tagged with oligonucleotides. These
274 oligonucleotides hybridize to connector oligonucleotides only if the antigens detected by the primary

275 antibodies are within ~40 nm of each other. Ligation of connector oligonucleotides and addition of a
276 polymerase results in rolling circle amplification to generate a sequence that can be detected by a
277 complementary oligonucleotide conjugated to a fluorescent probe (35). To determine whether PAV818
278 colocalizes with HIV-1 Gag, we performed biotin-Gag PLA on 293T cells that were chronically infected
279 with HIV-1 and treated with either PAV818, a biotinylated compound that lacks antiviral activity
280 (PAV543), or the DMSO vehicle (Fig 6A). Quantification of red fluorescent spots, which represent sites
281 where biotinylated compound and Gag are colocalized, revealed 5.8-fold more spots in cells treated with
282 the antiviral PAV818 than in cells treated with an equivalent concentration of the control compound
283 PAV543, and an even greater difference relative to DMSO treated cells (Fig 6B, C). Moreover, the
284 number of biotin-Gag spots observed with PAV818 treatment displayed a striking dose response
285 relationship (Fig 6B, C). Controls revealed that only a background level of spots was observed when
286 uninfected 293T cells were treated with PAV818, as would be expected given that uninfected cells lack
287 Gag (Fig 6B, C). Additionally, as expected, when antibody to biotin was replaced with a non-immune
288 control antibody only a few spots were observed; similar results were observed when antibody to Gag
289 was replaced with a non-immune control (Suppl Fig 1). Together these data indicate that PAV818
290 colocalizes with Gag in HIV-1 infected human cells.
291

292 **Drug-specific mutations were not observed in *gag* or *gagpol* after 37 weeks of selection with**
293 **PAV206**

294 The colocalization of PAV818 with HIV-1 Gag suggested a straightforward model in which Gag is
295 the target of this drug that appears to inhibit Gag assembly. If this is the case, then drug selection should
296 result in rapid acquisition of resistance mutations in the *gag* gene, analogous to what has been observed
297 for all antiretrovirals that target viral gene products. To determine if drug selection could identify a viral
298 target for this drug, we infected MT-2 T cells and passaged them under selection with PAV206 for 37
299 weeks, increasing the drug concentration by two-fold whenever evidence of resistance was observed,

300 and sequencing virus to score for dominant mutations periodically (Fig 7A, sequencing indicated by red
301 arrows). We also selected with the well-studied protease inhibitor Nelfinavir in parallel, as a positive
302 control.

303 Sequencing of virus under Nelfinavir selection revealed the emergence of three dominant non-
304 synonymous substitutions in HIV-1 protease: L90M, V77I, and L10F (indicated in red in Fig 7B; using
305 HXB2 genome numbering). All three are well-known Nelfinavir resistance mutations, with L90M being
306 a primary resistance mutation and V77I and L10F being common secondary mutations that further boost
307 resistance (36-40). The first two of these dominant resistance mutations emerged prior to passage 27,
308 just before the virus developed a high level of resistance, defined here as replication in a concentration
309 of Nelfinavir that is 16-fold higher than the EC50 (Nelfinavir P27 in Fig 7A, B). Two other
310 substitutions in Gag became dominant during Nelfinavir selection, A224T and H219Q (indicated in blue
311 in Fig 7B), at passage 21 and 29. H219Q and other substitutions in the cyclophilin A binding loop,
312 amino acids 217-225 in Gag, are polymorphisms found in the Los Alamos Database (41, 42)that are
313 known to reduce incorporation of cyclophilin A into virions when virus is passaged in cyclophilin-A-
314 rich immortalized CD4+T cells even in the absence of drugs, thereby resulting in virion cyclophilin A
315 levels that are optimal for replication in cyclophilin-A-rich cell lines (43, 44). Thus, from these data, we
316 infer that in the Nelfinavir selection group, tissue-culture-adaptive cyclophilin A binding loop
317 polymorphisms initially emerged in Gag and likely led to improved fitness and low-level resistance
318 (replication in a drug concentration 8-fold greater than the EC50); these were followed later by
319 Nelfinavir-specific resistance mutations, which likely led to high level Nelfinavir resistance.

320 Selection with PAV206 also led to emergence of dominant tissue-culture adaptive mutations. At
321 passage 19, virus from these cells had a V218M substitution in the cyclophilin A binding loop of Gag
322 (PAV206 P19 in Fig 7A, B). Like the cyclophilin A binding loop substitutions H219Q and A224T that
323 arose at passage 21 of Nelfinavir selection, V218M improves viral fitness in cyclophilin-A-rich CD4+ T
324 cells through reducing cyclophilin binding (41). However, unlike with Nelfinavir selection, no other

325 dominant non-synonymous mutations were observed in the *gag* or *gagpol* genes during 37 weeks of
326 selection with PAV206; moreover, high level resistance was also not observed (PAV206 in Fig 7A, B),
327 with passage in a PAV206 concentration that was 16-fold higher than the EC50 failing (J. Reed,
328 unpublished observations). Thus, selection with PAV206 did not result in drug-specific resistance
329 mutations in Gag, GagPol, or other viral genes, contrary to what might be expected for an assembly
330 inhibitor that directly targets a viral gene product.

331 Interestingly, dominant non-synonymous mutations in *env* were observed in both selection groups
332 (A541V, Q550H, and S144R in the Nelfinavir selection group, and N302Y, D547G, and Q550H in the
333 PAV206 selection group in Fig 7A, B). One of these mutations, A541V (observed at Nelfinavir P29 in
334 Fig 7A, B) was recently shown to confer broad escape from defects in virus replication defects caused
335 by either virus mutations or antiretroviral drugs, most likely by increasing cell-to-cell transmission in T
336 cell lines (45). The other dominant non-synonymous *env* mutations observed in our two selection
337 groups are likely to also be in this general category. Thus, while these *env* mutations are of interest, they
338 are not specific to PAV206 or any other drug – indeed, one of these mutations (Q550H) arose in both the
339 PAV206 and Nelfinavir selections (Fig 7A, B), underscoring that it is not drug-specific. Therefore, we
340 concluded that replication in PAV206 for 37 weeks failed to select for any drug-specific viral mutations
341 and therefore differed markedly from the Nelfinavir selection control, which demonstrated the classic
342 pattern of multiple resistance mutations emerging in the viral target of the drug. Consistent with this
343 conclusion, we observed a high level of resistance in the Nelfinavir selection group at passage 33 that
344 correlated with emergence of Nelfinavir-specific mutations in Pro, while resistance to PAV206 failed to
345 rise above the moderate level that is likely due to tissue-culture adaptation and mutations that confer and
346 global replication advantage in T cells.

347

348 **PAV206 colocalizes with host components of assembly intermediates, suggesting a host-targeting**
349 **mechanism**

350 Our studies to this point had shown that PAV206 colocalizes with Gag *in situ* (Fig 6) and appears to
351 inhibit Gag assembly (Fig 4), but unexpectedly does not appear to target Gag or GagPol based on
352 resistance studies (Fig 7). This led us to hypothesize that PAV206 and its analogs colocalizes with host
353 proteins as well as Gag, which would raise the possibility that PAV206 targets a host protein or viral-
354 host interface that is critical for assembly. This possibility is made more plausible by the fact that these
355 compounds were identified through assembly screens that recapitulate host-catalzyed capsid assembly
356 pathways. In the case of HIV-1 immature capsid assembly, two host proteins, ABCE1 and DDX6, are
357 known to promote assembly and are associated with Gag, serving as markers of Gag-containing
358 assembly intermediates (22, 26-30). Thus, we next used PLA to ask whether PAV206 colocalizes with
359 these Gag-associated host proteins.
360 293T cells chronically HIV-1 infected were treated with either PAV818, the biotinylated
361 antiretroviral compound, or PAV543, the biotinylated inactive compound, or DMSO and subjected to
362 biotin-ABCE1 PLA (Fig 8A). Quantification of red fluorescent spots representing sites where
363 biotinylated compound and ABCE1 are colocalized *in situ*, revealed 12.8-fold more spots in cells treated
364 with the antiviral PAV818 than in cells treated with an equivalent concentration of PAV543 or with
365 DMSO only (Fig 8B, C, 10 μM). Additionally, the number of biotin-ABCE1 spots observed with
366 PAV818 treatment displayed a striking dose response relationship (Fig 8B, C). Interestingly, PAV818
367 colocalized with ABCE1 even in uninfected 293T cells as well as HIV-1 infected human cells (Fig 8B,
368 C). As expected, controls in which antibody to biotin or to ABCE1 were individually replaced with a
369 non-immune control antibody revealed very few spots (Suppl Fig 2), as expected. PAV818 was also
370 found to colocalize with DDX6 in chronically HIV-1 infected 293T cells by PLA, with 5.2-fold more
371 spots observed in PAV818- vs. DMSO-treated cells (Fig 9). Thus, this novel antiretroviral compound
372 colocalizes with HIV-1 Gag as well as the host proteins ABCE1, and DDX6, all which are thought to be
373 components of HIV-1 assembly intermediates.
374

375 **Discussion**

376 Here we report our discovery of a family of small molecules, PAV206 and its analogs, that potently
377 inhibit HIV-1 replication by acting on intracellular viral late events, a stage of the viral life cycle that is
378 not specifically targeted by potent inhibitors currently in use or in development. Importantly, the exact
379 target and mechanism of action of this compound remain to be determined; however, the data from
380 virologic, resistance, and imaging studies presented here raise the intriguing possibility that this
381 compound does not specifically target a viral protein, but instead may target a host component of a
382 multi-protein complex that plays an important role in assembly of the immature HIV-1 capsid. While
383 further studies will be needed to test this hypothesis, PAV206 and its analogs should be of great interest
384 even at this early stage given that all existing antiretroviral drugs except one (CCR5 antagonists) target
385 viral proteins (direct-acting antivirals) and that host-targeting antivirals are highly desirable because they
386 offer a high genetic barrier to resistance that could allow us to win the drug resistance race (46, 47).

387 Most exciting in this regard was our observation that after selection with increasing concentrations
388 of PAV206 for 37 weeks in MT-2 T cells, sequence of replicating virus revealed no drug specific
389 mutations in Gag, GagPol, or any other viral gene product (Fig 7). Additionally, high level resistance to
390 PAV206 was not observed during this time (Fig 7). Such behavior is distinctly unusual, since all
391 existing classes of direct-acting antiretroviral drugs result in rapid development of resistance upon single
392 drug treatment. The unusual nature of this finding was emphasized by our finding that selection in
393 parallel with the protease inhibitor Nelfinavir resulted in three known resistance mutations in protease
394 during the 37-week selection as well as high-level resistance (allowing growth in drug concentrations
395 upto 16X higher than the EC50), as would be expected. Known tissue-culture adaptations were
396 observed in Gag, involving cyclophilin A loop polymorphisms, during PAV206 and Nelfinavir
397 selection. These polymorphisms are known to reduce the amount of cyclophilin A incorporated into
398 virions when virus is passaged in cyclophilin A-rich immortalized CD4+ T cells, in the presence or
399 absence of antiretroviral drugs (43, 44). Additionally, a second set of mutations was observed in

400 PAV206 and Nelfinavir. These mutations were in *env*, are not drug-specific, and have been shown to
401 confer global replication advantage most likely by increasing cell-to-cell transmission in T cell lines
402 (45). The modest resistance observed in the PAV206 selection experiment (allowing virus replication in
403 a PAV206 concentration 8X higher than the EC50) is likely explained by non-dominant cyclophilin A
404 binding loop polymorphisms and the *env* mutations that may have been emerging. In support of that
405 explanation, the appearance of modest resistance (to 8X EC50) in the Nelfinavir selection experiment
406 occurred around passage 20, correlated with emergence of a dominant cyclophilin A binding loop
407 polymorphism, and preceded the time when the drug-specific protease mutations became dominant.
408 While additional studies will be required to identify the target of PAV206, the surprising lack of
409 drug-specific viral resistance mutations raises the possibility that this compound acts on a host protein.
410 Two other observations are consistent with that hypothesis. First, this compound was identified using
411 novel screens that recapitulate host-catalyzed pathways in which assembling capsid proteins form a
412 series of host-protein containing assembly intermediates, culminating in formation of the completed
413 immature capsid. Such an assembly pathway screen was previously shown to identify a host-targeting
414 small molecule that potently inhibits rabies virus in cell culture (31). Second, our imaging studies show
415 that PAV206 colocalizes with Gag as well as two host enzymes, ABCE1 and DDX6 (Figs 6, 8, 9). Gag,
416 ABCE1, and DDX6 are components of intracellular assembly intermediates, which appear to be formed
417 when assembling HIV-1 Gag co-opts a host RNA-granule-like complex (20, 26-29). Future target
418 identification studies will be required to identify the direct target of PAV206, but based on data
419 presented here, we hypothesize that it may be a component of the RNA-granule-like assembly
420 intermediates.
421 PAV206 and its analogs are also of great interest because, to our knowledge, they are the first potent
422 small molecules shown to selectively inhibit late events in the HIV-1 life cycle. Unlike previously-
423 reported compounds that target CA, PAV117, a PAV206 analog, has no effects on viral early events,
424 and acts entirely on late events (Fig 3). Moreover, we showed that PAV117 dramatically reduces virus

425 production (Figs 3, 4), indicating that it acts on intracellular late events. PAV117 did not reduce steady
426 state levels of two cellular proteins, but did result in a modest reduction in steady state Gag levels. At
427 this point, we cannot rule out some effect on Gag synthesis; however, such an effect would be modest at
428 best given the significant levels of steady state Gag in our biochemical and imaging studies. We favor
429 the alternate hypothesis that the modest reductions in steady state Gag levels are due to degradation of
430 assembly intermediates that are associated with compound and therefore arrested. Consistent with this,
431 we observed a dose-dependent reduction in the proportion of Gag present in the final (~500S) assembly
432 intermediate but not in earlier assembly intermediates (~10S and ~80S/150S) (Fig 4). Nevertheless,
433 additional studies will be needed to determine the exact mechanism of action of PAV206 and its
434 analogs.

435 Finally, it should be noted that identification of these analogs constitutes an important validation of
436 the importance of HIV-1 RNA-granule-like assembly intermediates in virus production. remains
437 controversial. Surprisingly, the existence of assembly intermediates containing RNA granule proteins
438 continues to be questioned, even though numerous groups in addition to ours have implicated RNA
439 granule proteins as being important for assembly of diverse retroviruses and retroelements. For
440 example, knockout studies by the Sandmeyer group demonstrated that RNA granule proteins are
441 required for Ty3 retrotransposition in yeast and likely act during assembly (48-50). Additionally the
442 Linial group found that the RNA granule protein DDX6 is required for foamy virus packaging (51), and
443 the Mouland group showed that the RNA granule protein Stau1 plays an important role in HIV-1 Gag
444 assembly and packaging (52-55). Finally, the Kewalramani and Pathak groups demonstrated that RNA
445 granule protein MOV10 influences immature HIV-1 assembly (56, 57). Our finding of a potential first-
446 in-class family of small molecules that colocalize with host proteins in assembly intermediates and
447 likely act during immature capsid assembly supports the view that assembly intermediates not only exist
448 but are highly relevant to development of antiretroviral compounds that can be used to treat multidrug
449 resistant HIV-1 in the future.

450 **Materials and Methods**

451 **Plasmids:** The FIV-34TF10 ORFA+ proviral clone is described elsewhere. The NL4-3 clone was
452 obtained from NIH AIDs reagent program. The NL4-3 RLuc proviral clone was generated by replacing
453 *nef* with *Renilla* luciferase. We also generated a NL4-3 Rluc clone that is *env* deleted. FLUV WSN-33
454 isolate was obtained from Prosetta Biosciences. The NL4-3 Env construct used for psuedotyping was
455 codon optimized by IDT. The HIV-1 Q23.BG505 proviral clone (58)was obtained from Julie
456 Overbaugh.

457

458 **Cells and Transfection.** The feline astrocyte cell line G355-5 was obtained from ATCC (CRL-2033),
459 and maintained in McCoy 5A (modified) medium (Life Technologies, 16600-108) supplemented with
460 10% fetal bovine serum (Thermo Fisher, 26140079). Cells were transfected with 1 to 6 µg DNA in 6
461 cm dishes using X-treameGENE 9 (Roche, 6365787001). The 293T/17 cell line was obtained from
462 ATCC (CRL-11268), and maintained in DMEM media (Life Technologies, 10566-024) supplemented
463 with 10% fetal bovine serum (Thermo Fisher, 26140079). Chronically infected 293T are maintained
464 with DMEM supplemented with 0.5 µg/mL puromycin. Chronically infected H9 T cells are maintained
465 with cRPMI supplemented with 0.5 ug/mL puromycin. MT-2 cells (obtained from NIH AIDs reagents)
466 and SupT1.CCR5 cells (obtained from Julie Overbaugh) were maintained with cRPMI. MDCK.2 cells
467 (obtained from ATCC) are maintained in cMEM.

468

469 **Virus infectivity measurements.** Infectivity was measured by titering stocks on TZM-bl cells
470 (obtained from J.C. Kappes and X. Wu [University of Alabama, Birmingham, AL] and Tranzyme, Inc.
471 through the National Institutes of Health AIDS Research and Reference Reagent Program, Division of
472 AIDS, and National Institute of Allergy and Infectious Diseases). Infection of TZM-bl cells was
473 facilitated by the addition of 20 µg/ml DEAE dextran. Infectious units were determined by X-Gal
474 staining and counting blue cells. To determine relative infectivity, instead of X-Gal staining, a MUG (4-

475 methylumbelliferone β-D-galactopyranoside) substrate was used, and the change in MUG fluorescence
476 over time per volume of media was measured on a plate reader (Synergy; BioTek Instruments, Inc.) and
477 used to compare infectivity between samples.
478
479
480 **PBMC activation.** Thawed PBMC cells were pelleted by centrifugation 228xg for 8 minutes (Beckman
481 Allegra). Pellets were resuspended in stimulation media (cRPMI supplemented with 21 ng/mL hIL-2
482 [Peprotech] and 1.5 μg/mL PHA [Remel]) at a density of 2x10e6 cells/mL and transferred to T75 flask.
483 Cell were incubated for 3 days at 37°C in tissue culture incubator. After 3 day incubation cells were
484 collected and resuspended in iRPMI/20% FBS/10% DMSO and frozen down in 50x10e6 cells per vial.
485
486 **HIV virus production.** 293T/17 cells were seeded at 10x10e6 cells in T175 flask. Proviral constructs
487 were transfected with PEI. The next day cells were washed and cDMEM replenshied and return to 37°C
488 tissue cuture incubator. Media was collected at 48 and 72 hours post transfection. Media was filtered
489 0.45 micron PES membrane stored at -80°C as individual use aliqouts.
490
491 **FLUV virus production.** MDCK.2 cells were transferred with FLUV WSN-33 and incubated 37°C for
492 3 days. Media was collected tittered on MDCK.2 cells and stored at -80°C in individual use aliqouts.
493
494 **FIV virus production and RT assay.** G355-5 cells were transfected as described above but in 6-well
495 plates. Briefly, each well was transfected with 2 μg per well of FIV 34TF10 ORFA+ proviral plasmid.
496 At 24 hours post transfection cells were washed with media twice and media was replaced with 4 ml of
497 complete McCoy 5A. At 144 hours post transfection media was filtered with a 0.45 micron syringe
498 filter, aliquoted, and stored at -80C. Reverse transcriptase activity in media from FIV or mock
499 transfected cells was estimated using SG-PERT (59). A set of recombinant RT standards (EMD

500 Millipore catalog# 382129) ranging from 5.12e3 nU/mL to 5.12e9 nU/mL was used to estimate the
501 nU/mL of reverse transcriptase activity in the FIV stock.
502
503 **FIV inhibition assay.** Inhibition of FIV viral replication was assayed in a spreading infection using
504 G355-5 cells. G355-5 cells are seeded at 8000 cells/well in a 96-well polystyrene flat bottom tissue
505 culture plate one day before initiating assay to allow cells to adhere. Preparation and addition of
506 compounds followed the same procedure as the HIV-1 inhibition assay described above with the
507 following differences. For infection, 1954 nU RT activity of the FIV-34TF10 ORFA+ stock was used
508 per well. The spreading infection assays proceed for 144 hours. Infectious virus production was
509 measured by using the RT assay described above and cytotoxicity was determined following the same
510 procedure described under the HIV-1 inhibition assays.
511
512 **Inhibition of HIV-1 replication.** Inhibition of HIV-1 viral replication was assayed in a spreading
513 infection using MT-2 cells and NL4-3 *Renilla* Luciferase reporter virus or SupT1.CCR5 cells and HIV-1
514 Q23.BG505 virus. To obtain the compound dose-response curve, compounds are initially diluted with
515 DMSO to 100-times the starting concentration. Compounds are then further diluted 3-fold in DMSO
516 using 96-well round bottom polystyrene plates for a total of eight or nine dilutions. If a single
517 compound concentration was tested compound was diluted to 100-times the desired concentration in
518 DMSO. For the MT-2 assay, compound dilutions prepared above are then further diluted 50-fold with
519 cRPMI cRPMI with 400 IU/100 µL NL4-3 RLuc reporter virus. Then 100 µL of 50-fold diluted
520 compound is transferred to 20,000 MT-2 cells that were pre-seeded 96-well polystyrene flat bottom
521 tissue culture plates in 100 uL cRPMI for a final volume of 200 uL. The final MOI in infected plates is
522 0.02 and the final DMSO concentration in all wells is 1%. For each replicate one well receives DMSO
523 only and one well receives media only for normalization and background correction. All assays are run
524 with three replicates. Plates are then incubated for 96 hours 37°C in a tissue culture incubator. To assay

525 inhibition of HIV-1 replication 100 µL of media was removed and discarded and 10 µL of 15 µM
526 EnduRen stock was added to each well. Plates were then incubated for 1.5 hours at 37°C in a tissue
527 culture incubator. Following incubation plates were mixed well and read on Luminescence plate reader
528 (Synergy; BioTek Instruments, Inc.). The HIV-1 inhibition assay using SupT1.CCR5 cells and
529 Q23.BG505 virus stock, followed a similar protocol with the following exceptions. First, 12.5 uL of
530 Q23.BG505 virus stock was used per well, an amount optimized to provide linear signal over a 96-hour
531 spreading infection. Second, inhibition of HIV-1 replication was determined by measuring the relative
532 infectivity produced form infected cells by MUG assay (see virus infectivity measurements) instead of
533 the luciferase endpoint. The HIV-1 inhibition assay using PBMC cells, followed a similar protocol with
534 the following exceptions. Frozen activated PBMC cells were thawed and resuspended in PBMC media
535 (cRPMI supplemented with 21 ng/mL hIL-2 [Peprotech]) at 0.5x10e6 cells/mL for 3 days in 37°C tissue
536 culture incubator. Cells were collected and adjusted to 2x10e6 cells/mL in PBMC media and bulk
537 infected for 2 hours at a MOI 0.008 with NL4-3 virus stock at 37°C. Compound dilutions were prepared
538 as above in cRPMI and 100 uL of diluted compound was transferred to 96-well U bottom polystyrene
539 tissue culture plates. Bulk infected cells were pelleted and resuspended in PBMC media at 1x10e6
540 cells/mL at 100 µL of cell suspension per well was transferred to assay plate for 100,000 cells per well.
541 96 hpi media was collected for relative infectivity measurements as was done with SupT1.CCR5 assay.
542
543 **MT-2 acute infection assay.** MT-2 cells were diluted to 2x10e6 cells/mL with cRPMI and bulk
544 infected at an MOI 1 for 2 hours at 37°C in tissue culture incubator. Cells were washed three times with
545 cRPMI to remove inoculum. Compound and DMSO was diluted in media and added to 12-well
546 polystyrene tissue culture plate in 1 mL volume. Then 1 mL of 0.5x10e6 infected MT-2 cells were then
547 added. Forty-eight hours later media was collected for virus pelleting by ultracentrifugation and cells
548 were washed and harvested with 1xLSM buffer.
549

550 **Inhibition of HIV-1 early events.** To assess inhibition of HIV-1 early events the HIV-1 inhibition
551 procedure for MT-2 described above was followed with the following exceptions. MT-2 cells were
552 infected with 0.5 μL of HIV-1 NL4-3 *Renilla* luciferase reporter virus that was *env* deleted and
553 psuedotyped with NL4-3 Env stock per well, an amount optimized to provide sufficient signal. Lastly,
554 the luciferase endpoint was collected at 48 hours instead of 96 hours.
555
556 **Inhibition of HIV-1 late events.** To assess inhibition of HIV-1 late events the HIV-1 inhibition
557 procedure for MT-2 described above was followed with the following exceptions. Here an H9
558 chronically infected T cell line was utilized instead of acute infection in MT-2 cells and inhibition of
559 infectious virus production was assayed by collecting media and measuring relative infectivity produced
560 form infected cells by MUG assay (see virus infectivity measurements). Inhibition of virus production
561 was assayed by analyzing PEG pelleted virus by WB with αGag.
562
563 **FLUV antiviral assay.** Inhibition of FLUV was assayed using infection of MDCK.2 cells. First,
564 MDCK.2 cells were seeded in a 96-well polystyrene tissue culture plate at 30,000 cells/well. The next
565 day they were infected with FLUV WSN-33 at an MOI of 0.001 for 1 hour at 37°C in tissue culture
566 incubator. After 1 hour incubation cells were washed three times with PBS and 90 uL of cMEM added
567 to cells. Single compound dilutions were prepared in cMEM at 10x the desired final concentration in
568 the inhibition assay. Either 10 μL of DMSO or 10x compound was added to infected cells for final
569 volume of 100 μL. To prepare for TCID50 measurements the following day MDCK.2 cells are seeded
570 at 30,000 cells/well in a 96-well polystyrene flat bottom tissue culture plate. The following day, ~24
571 hpi, media is collected from infected treated cells and 10^{-1}-10^{-6} dilutions are prepared and used to infect
572 MDCK.2 cells seeded the day prior. This plate is returned to 37°C tissue culture incubator for 3 days.
573 After 3 days, infected loci are counted and used to calculate TCID50/mL.
574

575 **Cytotoxicity Assays**: For each viral inhibition assay a parallel cytotoxicity assay was setup following
576 the same procedure except virus was not added. Cytotocity was assessed at the same time the viral
577 inhibition assays by adding 20 µL of AlamarBlue to the cytotoxicity plates and mixed well with cells.
578 AlamarBlue treated plates were then incubated for 2-3 hours at 37°C in a tissue culture incubator (timing
579 was optimized for linear signal), mixed well again, and then read on fluorescence plate reader (Synergy;
580 BioTek Instruments, Inc.).
581
582 **Virus Pelleting.** For the dose-response assay shown in Fig 3B, culture supernatants were collected at 48
583 hours and virus pelleted by PEG precipitation. First, 75 µL of 17% PEG 6000/0.8M NaCl/PBS was
584 added 96-well V-bottom polypropylene plate followed by 75 µL media from the assay plate. PEG and
585 media are mixed well then incubated on ice for 2 hours or overnight at 4°C. Virus is then pelleted
586 1847xg in SX4750 rotor in Beckman Allegra Centrifuge 4°C. Media and PEG solution is aspirated and
587 pellet resuspended in 50 uL loading buffer with DTT. For Fig 4, culture supernatants were collected 48
588 hours post infection and filtered with 0.45 micron PES syringe filter to remove any remaining cells.
589 Virus-like particles were centrifuged through a 30% w/v sucrose/PBS cushion (Beckman SW55Ti,
590 130,000xg, 30 minutes, 4C). The virus pellet was harvested directly for analysis by WB with an
591 antibody to HIV-1 Gag.
592
593 **Proximity Ligation Assay (PLA)** 293T/17 cells or chronically infected 293T cells were plated into 6-
594 well dishes containing poly-L-lysine-coated coverslips with Grace Biolabs CultureWell silicone
595 chambers (Sigma-Aldrich) attached to create four chambers on each coverslip. Cells were treated with
596 compound, DMSO, or left untreated and 16 hours later were fixed for 15 minutes in 4%
597 paraformaldehyde in PBS pH 7.4, permeabilized in 0.5% w/v Saponin in PBS, pH 7.4 for 10 minutes,
598 and blocked in Duolink blocking solution (Sigma-Aldrich) at 37°C for at least 30 min. Cells were
599 incubated in primary antibody (described under antibodies), followed by Duolink reagents (Sigma-

600 Aldrich): oligo-linked secondary antibody, ligation mix, and red amplification/detection mix, with
601 washes in between, as per the Duolink protocol. For concurrent immunofluorescence (IF), cells were
602 incubated for 30 minutes at RT with 1:1000 Alexafluor 488 anti-mouse secondary antibody following
603 the final 1x Buffer B PLA washes. Cover slips were mounted using Duolink In Situ Mounting Media
604 with DAPI, sealed to the glass slides with clear nail polish, allowed to dry for 24 h at RT, and stored at -
605 20°C. Imaging was performed with a Zeiss Axiovert 200M deconvolution microscope using Zeiss Plan-
606 Apochromat 63X/ aperture 1.4 objective with oil immersion, with AxioVision Rel. 4.8 software. For
607 quantification, five to ten fields containing at least three IF-positive cells were chosen at random and
608 imaged using identical exposure times for the red and green channels (red/green exposures were 100 ms
609 second and 500 ms seconds, respectively). Images were captured as a Z-stack of 80-90 0.27-µm slices
610 to capture the entire cell body (~10 µM). Images were deconvolved using the AxioVision software, then
611 central Z-stack image was exported as tif files, and Image J was used to outline Gag-positive cells in
612 each field. Within those IF positive cells, the central Z-stack image was used to count the number of
613 PLA "spots", and quantify IF intensity where indicated, using Image J. PLA spot number for each field
614 was then normalized to the average IF intensity within that field, and the results were plotted with error
615 bars representing the SEM for five fields. Prior to export of the images used in the figures, the gain on
616 all red channels was adjusted to 3 in the AxioVision software to allow spots to be easily seen by eye.
617 Images were then imported in 8-bit color into Adobe Illustrator to create the final figure layout, without
618 further adjustments to color balance or gamma correction. Images shown in figures display an image
619 from the center slice of a Z-stack that is representative of the mean. Experiment was repeated once, with
620 similar results.
621
622
623
624

Acknowledgments

The following reagents were obtained through the NIH AIDS Reagent Program, Division of AIDS, NIAID, NIH: anti-HIV-1 p24 hybridoma antibody (183-H12-5C) from Bruce Chesebro and Hardy Chen. HIV-1 Q23.BG505 virus and SupT1.CCR5 cells were obtained from Dr. Julie Overbaugh. We acknowledge Michael Emerman for advice.

Jaisri R. Lingappa and Jonathan C. Reed have shares or stock options in Prosetta Biosciences, and Jaisri R. Lingappa receives some unrestricted research funding from Prosetta Biosciences. VRL is CEO and Scientific Director of Prosetta Biosciences.

These studies were funded by NIH R01AI150457, NIH R56 AI145498, and Prosetta Biosciences. Neither of the funders (NIH or Prosetta Biosciences) had any role in study design, data collection and interpretation, or the decision to submit the work for publication.

650 **References**

651 1. Abner E, Jordan A. 2019. HIV "shock and kill" therapy: In need of revision. Antiviral Res
652 166:19-34.
653 2. Pham HT, Mesplede T. 2018. The latest evidence for possible HIV-1 curative strategies. Drugs
654 Context 7:212522.
655 3. Collier DA, Monit C, Gupta RK. 2019. The Impact of HIV-1 Drug Escape on the Global
656 Treatment Landscape. Cell Host Microbe 26:48-60.
657 4. Boender TS, Sigaloff KC, McMahon JH, Kiertiburanakul S, Jordan MR, Barcarolo J, Ford N,
658 Rinke de Wit TF, Bertagnolio S. 2015. Long-term Virological Outcomes of First-Line
659 Antiretroviral Therapy for HIV-1 in Low- and Middle-Income Countries: A Systematic Review
660 and Meta-analysis. Clin Infect Dis 61:1453-61.
661 5. Gregson J, Kaleebu P, Marconi VC, van Vuuren C, Ndembi N, Hamers RL, Kanki P, Hoffmann
662 CJ, Lockman S, Pillay D, de Oliveira T, Clumeck N, Hunt G, Kerschberger B, Shafer RW, Yang
663 C, Raizes E, Kantor R, Gupta RK. 2017. Occult HIV-1 drug resistance to thymidine analogues
664 following failure of first-line tenofovir combined with a cytosine analogue and nevirapine or
665 efavirenz in sub Saharan Africa: a retrospective multi-centre cohort study. Lancet Infect Dis
666 17:296-304.
667 6. Cambiano V, Bertagnolio S, Jordan MR, Pillay D, Perriens JH, Venter F, Lundgren J, Phillips A.
668 2014. Predicted levels of HIV drug resistance: potential impact of expanding diagnosis,
669 retention, and eligibility criteria for antiretroviral therapy initiation. AIDS 28 Suppl 1:S15-23.
670 7. Llibre JM. 2017. Time to get serious with HIV-1 resistance in sub-Saharan Africa. Lancet Infect
671 Dis 17:241-243.
672 8. Dionne B. 2019. Key Principles of Antiretroviral Pharmacology. Infect Dis Clin North Am
673 33:787-805.

674 9. Carnes SK, Sheehan JH, Aiken C. 2018. Inhibitors of the HIV-1 capsid, a target of opportunity.
675 Curr Opin HIV AIDS 13:359-365.
676 10. Thenin-Houssier S, Valente ST. 2016. HIV-1 Capsid Inhibitors as Antiretroviral Agents. Curr
677 HIV Res 14:270-82.
678 11. Balasubramaniam M, Zhou J, Addai A, Martinez P, Pandhare J, Aiken C, Dash C. 2019. PF74
679 Inhibits HIV-1 Integration by Altering the Composition of the Preintegration Complex. J Virol
680 93.
681 12. Bhattacharya A, Alam SL, Fricke T, Zadrozny K, Sedzicki J, Taylor AB, Demeler B, Pornillos
682 O, Ganser-Pornillos BK, Diaz-Griffero F, Ivanov DN, Yeager M. 2014. Structural basis of HIV-
683 1 capsid recognition by PF74 and CPSF6. Proc Natl Acad Sci U S A 111:18625-30.
684 13. Rankovic S, Ramalho R, Aiken C, Rousso I. 2018. PF74 Reinforces the HIV-1 Capsid To Impair
685 Reverse Transcription-Induced Uncoating. J Virol 92.
686 14. Shi J, Zhou J, Shah VB, Aiken C, Whitby K. 2011. Small-molecule inhibition of human
687 immunodeficiency virus type 1 infection by virus capsid destabilization. J Virol 85:542-9.
688 15. Zhou J, Price AJ, Halambage UD, James LC, Aiken C. 2015. HIV-1 Resistance to the Capsid-
689 Targeting Inhibitor PF74 Results in Altered Dependence on Host Factors Required for Virus
690 Nuclear Entry. J Virol 89:9068-79.
691 16. Yant SR, Mulato A, Hansen D, Tse WC, Niedziela-Majka A, Zhang JR, Stepan GJ, Jin D, Wong
692 MH, Perreira JM, Singer E, Papalia GA, Hu EY, Zheng J, Lu B, Schroeder SD, Chou K,
693 Ahmadyar S, Liclican A, Yu H, Novikov N, Paoli E, Gonik D, Ram RR, Hung M, McDougall
694 WM, Brass AL, Sundquist WI, Cihlar T, Link JO. 2019. A highly potent long-acting small-
695 molecule HIV-1 capsid inhibitor with efficacy in a humanized mouse model. Nat Med 25:1377-
696 1384.
697 17. Blair WS, Pickford C, Irving SL, Brown DG, Anderson M, Bazin R, Cao J, Ciaramella G,
698 Isaacson J, Jackson L, Hunt R, Kjerrstrom A, Nieman JA, Patick AK, Perros M, Scott AD,

699 Whitby K, Wu H, Butler SL. 2010. HIV capsid is a tractable target for small molecule
700 therapeutic intervention. PLoS Pathog 6:e1001220.
701 18. Lemke CT, Titolo S, Goudreau N, Faucher AM, Mason SW, Bonneau P. 2013. A novel
702 inhibitor-binding site on the HIV-1 capsid N-terminal domain leads to improved crystallization
703 via compound-mediated dimerization. Acta Crystallogr D Biol Crystallogr 69:1115-23.
704 19. Bush DL, Vogt VM. 2014. In Vitro Assembly of Retroviruses. Annu Rev Virol 1:561-80.
705 20. Barajas BC, Tanaka M, Robinson BA, Phuong DJ, Chutiraka K, Reed JC, Lingappa JR. 2018.
706 Identifying the assembly intermediate in which Gag first associates with unspliced HIV-1 RNA
707 suggests a novel model for HIV-1 RNA packaging. PLoS Pathog 14:e1006977.
708 21. Dooher JE, Lingappa JR. 2004. Conservation of a step-wise, energy-sensitive pathway involving
709 HP68 for assembly of primate lentiviral capsids in cells. J Virol 78:1645-56.
710 22. Dooher JE, Schneider BL, Reed JC, Lingappa JR. 2007. Host ABCE1 is at Plasma Membrane
711 HIV Assembly Sites and Its Dissociation from Gag is Linked to Subsequent Events of Virus
712 Production. Traffic 8:195-211.
713 23. Klein KC, Reed JC, Tanaka M, Nguyen VT, Giri S, Lingappa JR. 2011. HIV Gag-leucine zipper
714 chimeras form ABCE1-containing intermediates and RNase-resistant immature capsids similar
715 to those formed by wild-type HIV-1 Gag. J Virol 85:7419-35.
716 24. Lingappa JR, Hill RL, Wong ML, Hegde RS. 1997. A multistep, ATP-dependent pathway for
717 assembly of human immunodeficiency virus capsids in a cell-free system. J Cell Biol 136:567-
718 81.
719 25. Lingappa JR, Newman MA, Klein KC, Dooher JE. 2005. Comparing capsid assembly of primate
720 lentiviruses and hepatitis B virus using cell-free systems. Virology 333:114-23.
721 26. Reed JC, Molter B, Geary CD, McNevin J, McElrath J, Giri S, Klein KC, Lingappa JR. 2012.
722 HIV-1 Gag co-opts a cellular complex containing DDX6, a helicase that facilitates capsid
723 assembly. J Cell Biol 198:439-56.

724 27. Reed JC, Westergreen N, Barajas BC, Ressler DTB, Phuong DJ, Swain JV, Lingappa VR,
725 Lingappa JR. 2018. The formation of RNA granule-derived capsid assembly intermediates
726 appears to be conserved between HIV-1 and the non-primate lentivirus FIV. J Virol
727 doi:10.1128/JVI.01761-17.
728 28. Robinson BA, Reed JC, Geary CD, Swain JV, Lingappa JR. 2014. A temporospatial map that
729 defines specific steps at which critical surfaces in the Gag MA and CA domains act during
730 immature HIV-1 capsid assembly in cells. J Virol 88:5718-41.
731 29. Tanaka M, Robinson BA, Chutiraka K, Geary CD, Reed JC, Lingappa JR. 2015. Mutations of
732 Conserved Residues in the Major Homology Region Arrest Assembling HIV-1 Gag as a
733 Membrane-Targeted Intermediate Containing Genomic RNA and Cellular Proteins. J Virol
734 90:1944-63.
735 30. Zimmerman C, Klein KC, Kiser PK, Singh ARS, Firestein BL, Riba SC, Lingappa JR. 2002.
736 Identification of a host protein essential for assembly of immature HIV-1 capsids. Nature
737 415:88-92.
738 31. Lingappa UF, Wu X, Macieik A, Yu SF, Atuegbu A, Corpuz M, Francis J, Nichols C, Calayag
739 A, Shi H, Ellison JA, Harrell EK, Asundi V, Lingappa JR, Prasad MD, Lipkin WI, Dey D, Hurt
740 CR, Lingappa VR, Hansen WJ, Rupprecht CE. 2013. Host-rabies virus protein-protein
741 interactions as druggable antiviral targets. Proceedings of the National Academy of Sciences of
742 the United States of America 110:E861-8.
743 32. Freienstein C, Blobel G. 1974. Use of eukaryotic native small ribosomal subunits for the
744 translation of globin messenger RNA. Proc Natl Acad Sci U S A 71:3435-9.
745 33. Singh AR, Hill RL, Lingappa JR. 2001. Effect of mutations in Gag on assembly of immature
746 human immunodeficiency virus type 1 capsids in a cell-free system. Virology 279:257-70.

747 34. Lingappa JR, Dooher JE, Newman MA, Kiser PK, Klein KC. 2006. Basic residues in the
748 nucleocapsid domain of Gag are required for interaction of HIV-1 gag with ABCE1 (HP68), a
749 cellular protein important for HIV-1 capsid assembly. J Biol Chem 281:3773-84.
750 35. Soderberg O, Gullberg M, Jarvius M, Ridderstrale K, Leuchowius KJ, Jarvius J, Wester K,
751 Hydbring P, Bahram F, Larsson LG, Landegren U. 2006. Direct observation of individual
752 endogenous protein complexes in situ by proximity ligation. Nat Methods 3:995-1000.
753 36. Gupta A, Jamal S, Goyal S, Jain R, Wahi D, Grover A. 2015. Structural studies on molecular
754 mechanisms of Nelfinavir resistance caused by non-active site mutation V77I in HIV-1 protease.
755 BMC Bioinformatics 16 Suppl 19:S10.
756 37. Perry CM, Frampton JE, McCormack PL, Siddiqui MA, Cvetkovic RS. 2005. Nelfinavir: a
757 review of its use in the management of HIV infection. Drugs 65:2209-44.
758 38. Rhee SY, Gonzales MJ, Kantor R, Betts BJ, Ravela J, Shafer RW. 2003. Human
759 immunodeficiency virus reverse transcriptase and protease sequence database. Nucleic Acids
760 Res 31:298-303.
761 39. Rhee SY, Taylor J, Wadhera G, Ben-Hur A, Brutlag DL, Shafer RW. 2006. Genotypic predictors
762 of human immunodeficiency virus type 1 drug resistance. Proc Natl Acad Sci U S A 103:17355-
763 60.
764 40. Weber IT, Agniswamy J. 2009. HIV-1 Protease: Structural Perspectives on Drug Resistance.
765 Viruses 1:1110-36.
766 41. Gatanaga H, Das D, Suzuki Y, Yeh DD, Hussain KA, Ghosh AK, Mitsuya H. 2006. Altered
767 HIV-1 Gag protein interactions with cyclophilin A (CypA) on the acquisition of H219Q and
768 H219P substitutions in the CypA binding loop. J Biol Chem 281:1241-50.
769 42. Kuiken C, Foley B, Hahn B, Marx P, McCutchan F, Mellors JW, Mullins J, Wolinsky S, Korber
770 B. 2000. Human Retroviruses and AIDS Los Alamaos National Laboratory, Los Alamos, NM.

771 43. Dicker I, Zhang S, Ray N, Beno BR, Regueiro-Ren A, Joshi S, Cockett M, Krystal M, Lataillade
772 M. 2019. Resistance profile of the HIV-1 maturation inhibitor GSK3532795 in vitro and in a
773 clinical study. PLoS One 14:e0224076.
774 44. Gatanaga H, Suzuki Y, Tsang H, Yoshimura K, Kavlick MF, Nagashima K, Gorelick RJ, Mardy
775 S, Tang C, Summers MF, Mitsuya H. 2002. Amino acid substitutions in Gag protein at non-
776 cleavage sites are indispensable for the development of a high multitude of HIV-1 resistance
777 against protease inhibitors. J Biol Chem 277:5952-61.
778 45. Van Duyne R, Kuo LS, Pham P, Fujii K, Freed EO. 2019. Mutations in the HIV-1 envelope
779 glycoprotein can broadly rescue blocks at multiple steps in the virus replication cycle. Proc Natl
780 Acad Sci U S A 116:9040-9049.
781 46. Garbelli A, Riva V, Crespan E, Maga G. 2017. How to win the HIV-1 drug resistance hurdle
782 race: running faster or jumping higher? Biochem J 474:1559-1577.
783 47. Ji X, Li Z. 2020. Medicinal chemistry strategies toward host targeting antiviral agents. Med Res
784 Rev doi:10.1002/med.21664.
785 48. Beliakova-Bethell N, Beckham C, Giddings TH, Jr., Winey M, Parker R, Sandmeyer S. 2006.
786 Virus-like particles of the Ty3 retrotransposon assemble in association with P-body components.
787 RNA 12:94-101.
788 49. Bilanchone V, Clemens K, Kaake R, Dawson AR, Matheos D, Nagashima K, Sitlani P, Patterson
789 K, Chang I, Huang L, Sandmeyer S. 2015. Ty3 Retrotransposon Hijacks Mating Yeast RNA
790 Processing Bodies to Infect New Genomes. PLoS Genet 11:e1005528.
791 50. Irwin B, Aye M, Baldi P, Beliakova-Bethell N, Cheng H, Dou Y, Liou W, Sandmeyer S. 2005.
792 Retroviruses and yeast retrotransposons use overlapping sets of host genes. Genome Res 15:641-
793 54.
794 51. Yu S, Lujan P, Jackson D, Emerman M, Linial M. 2011. The DEAD-box RNA helicase DDX6 is
795 required for efficient encapsidation of a retroviral genome. PloS Pathog 7:e1002303.

796 52. Abrahamyan LG, Chatel-Chaix L, Ajamian L, Milev MP, Monette A, Clement JF, Song R,
797 Lehmann M, DesGroseillers L, Laughrea M, Boccaccio G, Mouland AJ. 2010. Novel Staufen1
798 ribonucleoproteins prevent formation of stress granules but favour encapsidation of HIV-1
799 genomic RNA. J Cell Sci 123:369-83.
800 53. Chatel-Chaix L, Abrahamyan L, Frechina C, Mouland AJ, DesGroseillers L. 2007. The host
801 protein Staufen1 participates in human immunodeficiency virus type 1 assembly in live cells by
802 influencing pr55Gag multimerization. J Virol 81:6216-30.
803 54. Chatel-Chaix L, Boulay K, Mouland AJ, Desgroseillers L. 2008. The host protein Staufen1
804 interacts with the Pr55Gag zinc fingers and regulates HIV-1 assembly via its N-terminus.
805 Retrovirology 5:41.
806 55. Rao S, Hassine S, Monette A, Amorim R, DesGroseillers L, Mouland AJ. 2019. HIV-1 requires
807 Staufen1 to dissociate stress granules and to produce infectious viral particles. RNA 25:727-736.
808 56. Burdick R, Smith JL, Chaipan C, Friew Y, Chen J, Venkatachari NJ, Delviks-Frankenberry KA,
809 Hu WS, Pathak VK. 2010. P body-associated protein Mov10 inhibits HIV-1 replication at
810 multiple stages. J Virol 84:10241-53.
811 57. Furtak V, Mulky A, Rawlings SA, Kozhaya L, Lee K, Kewalramani VN, Unutmaz D. 2010.
812 Perturbation of the P-body component Mov10 inhibits HIV-1 infectivity. PloS one 5:e9081.
813 58. Dingens AS, Haddox HK, Overbaugh J, Bloom JD. 2017. Comprehensive Mapping of HIV-1
814 Escape from a Broadly Neutralizing Antibody. Cell Host Microbe 21:777-787 e4.
815 59. Vermeire J, Naessens E, Vanderstraeten H, Landi A, Iannucci V, Van Nuffel A, Taghon T,
816 Pizzato M, Verhasselt B. 2012. Quantification of reverse transcriptase activity by real-time PCR
817 as a fast and accurate method for titration of HIV, lenti- and retroviral vectors. PLoS One
818 7:e50859.
819
820

821 **Figure Legends**

822 **Fig 1: The HIV-1 assembly pathway and HIV-1 assembly drug screen.** (A) Diagram of the HIV-1
823 lifecycle starting with the integrated provirus in an infected cell on the left-hand side of the panel and
824 proceeding through the late and early phases of the lifecycle ending with integration in a newly infected
825 cell on the right-hand side of the panel. The different stages of the lifecycle are indicated beneath the
826 diagram either in black text or in blue text if that step is a target of one of the ART compounds shown.
827 Select antiretroviral compounds currently used for ART are shown in blue text and where they act on the
828 HIV-1 lifecycle is indicated. (B) Diagram of the host-catalyzed HIV-1 assembly pathway starting with
829 synthesis of Gag forming the early ~10S assembly intermediate and ending with formation of the ~750S
830 completed immature capsid. (C) Diagram showing the cell-free assembly plate screen that was utilized
831 to identify small compounds that inhibit the host-catalyzed pathway of HIV-1 assembly. Diagram in the
832 upper part of panel (C) shows detection of both early and late assembly intermediates from an HIV-1
833 cell-free assembly reaction carried out in the presence of DMSO only, which does not inhibit assembly.
834 Diagram in the lower part of panel (C) shows the effect of a compound that inhibits HIV-1 capsid
835 assembly in the cell-free assembly reaction, resulting in reduced detection relative to the DMSO control.
836

837 **Fig 2: PAV-117, identified in a cell-extract-based assembly screen, inhibits replication of HIV-1,**
838 **but not FIV and FLUV, in cell culture.** (A) The chemical structure of PAV117. (B) Dose-response
839 curve for PAV117 inhibition of HIV-1 replication was generated by treatment of MT-2 cells with
840 various doses of PAV117 followed by infection with HIV-1 NL4-3 *Renilla* luciferase reporter virus at a
841 MOI 0.02. HIV-1 replication proceeded for 96 hours followed by luciferase activity measurement,
842 which was used to calculate %inhibition relative to DMSO-treated controls. The 50% effective
843 concentration (EC50) is shown in blue on the dose-response plot. The 50% cytotoxicity concentration
844 (CC50), which was determined in parallel using uninfected MT-2 T cells, is shown in black and the
845 concentration marked by a vertical dashed line on the plot. Standard errors determined from three

846 replicates are shown. (C) Quantification of FLUV WSN-33 viral titer (TCID50) produced over 24 hours
847 from MDCK cells treated with 0.8 μM PAV117, 10 μM Tamiflu, or DMSO followed by infection with
848 FLUV WSN-33 at a MOI 0.001. (D) Dose-response curve for PAV117 inhibition of FIV replication
849 was generated by treatment of G355-5 cells with various doses of PAV117 followed by infection with
850 FIV 34TF10 with 1954 nU of RT activity per well. FIV replication proceeded for 144 hours followed
851 by RT measurement, which was used to calculate %inhibition relative to DMSO controls. The EC50 is
852 shown in purple on the dose-response plot. The CC50, which was determined in parallel using
853 uninfected G355-5 cells, is shown in black and the concentration marked by a vertical dashed line on the
854 plot. Standard errors determined from three replicates are shown. (E) Quantification of HIV-1
855 replication in SupT1.CCR5 cells treated with 0.37 μM PAV117 or DMSO followed by infection with
856 HIV-1 Q23. HIV-1 replication proceeded for 96 hours followed HIV-1 infectivity measurement of the
857 culture supernatant utilizing the MUG assay and the Tzm-bl indicator cell line. Standard errors
858 determined from three replicates are shown.
859
860 **Fig. 3: PAV-117 acts late in the HIV-1 life cycle, inhibiting virus production but not specific**
861 **infectivity.** (A) Schematic of the early assay protocol. The early assay starts with infection of MT-2
862 cells with HIV-1 NL4-3 *Renilla* Luciferase reporter virus in the presence of compound or DMSO. The
863 reporter virus used in the early assay is envelope deleted and psuedotyped with HIV-1 NL4-3 Env, thus
864 is restricted to a single round of infection. After 48 hours luciferase activity is measured and used to
865 calculate percent inhibition relative to the DMSO control. The assay measures effects only on entry to
866 early viral gene expression. Below the schematic is a dose-response curve for PAV117 inhibition of the
867 early events of the HIV-1 lifecycle generated with various doses of PAV117 in the early assay described
868 above. The 50% effective concentration (EC50) is shown in red on the dose response plot. The 50%
869 cytotoxic concentration (CC50), which was determined in parallel using uninfected MT-2 T cells, is
870 shown in black and the concentration marked by a vertical dashed line on the plot. Standard errors

871 determined from three replicates is shown. (B) Schematic of late assay protocol. The late assay starts
872 with chronically infected H9 T cells (H9-HIV) that are treated with either compound or DMSO and 48
873 hours later media is collected. The media is used to titer HIV-1 infectivity on an indicator cell line
874 (Tzm-bl) or virus was pelleted and assayed by western blot (WB) with an antibody directed against
875 HIV-1 Gag (αGag). These measurements are used to calculate percent inhibition relative to DMSO.
876 The late assay measures effects only on early viral gene expression to viral maturation. Below the
877 schematic is a dose-response curve for PAV117 inhibition of the late events of the HIV-1 lifecycle
878 generated with various doses of PAV117 in the late assay described above. The blue dose-response
879 curve shows inhibition of PAV117 on virus production as determined by WB of virus pellets with αGag.
880 The EC50 of PAV117 on virus production is shown in blue text on the dose-response plot. WB of virus
881 pellets with αGag is shown beneath the dose-response plot (one representative replicate is shown).
882 Treatment with DMSO or the concentration of PAV117 is shown above the WB. Percent inhibition
883 relative to DMSO based on quantification from the WB is shown beneath the WB. The black dose-
884 response curve shows inhibition of PAV117 on HIV-1 infectivity. The EC50 of PAV117 on HIV-1
885 infectious virus production is shown in black text on the dose-response curve. The CC50, which was
886 determined on the H9-HIV cells, is shown in black and the concentration marked by a vertical dashed
887 line on the plot. For each dose-response plot standard errors determined from three replicates is shown.
888

889 **Fig. 4: PAV-117 acts during the HIV-1 assembly pathway, after formation of the ~80S**
890 **intermediate.** Infected MT-2 cells were treated with the PAV117 or DMSO for forty-eight hours and
891 media was collected to analyze effects on (A, left-hand bar graph) virus production, (A, right-hand bar
892 graph) intracellular Gag steady-state levels, (B) intracellular level of two housekeeping proteins,
893 GAPDH and actin, and (C) intracellular steady-state levels of assembly intermediates. To evaluate
894 effects of PAV117 on virus production, virus was pelleted from media of treated cells and pellets were
895 analyzed by western blot (WB) with an antibody directed against HIV-1 p24 Gag (αGag).

896 Quantification of p24 Gag in virus pellets from WB data is shown as percent relative to the DMSO
897 control in the left-hand bar graph of panel (A) with specific treatments indicated beneath the bar graph.
898 A representative WB from one replicate is shown beneath the bar graph with the expected migration of
899 p24 Gag indicated to the right of the WB. To evaluate effect of PAV117 treatments on intracellular
900 steady state p55 Gag level, cell lysates were analyzed by WB with αGag. Quantification of p55 Gag in
901 cell lysates from WB data is shown as percent relative to DMSO control in the right-hand bar graph of
902 panel (A), with specific treatment indicated beneath the bar graph. A representative WB from one
903 replicate is shown beneath the bar graph with the expected migration of p55 Gag indicated to the right of
904 the WB. To evaluate effects of PAV117 on intracellular steady-state levels of GAPDH or Actin, cell
905 lysates analyzed in panel (A), were also subjected to WB with an antibody directed against GAPDH
906 (αGAPDH) or actin (αactin). Quantification of GAPDH or actin in cell lysates from WB data is shown
907 as percent relative to DMSO control in panel (B), with the specific treatment indicated beneath the bar
908 graph. A representative WB for each housekeeping protein from one replicate is shown beneath the bar
909 graph with the expected migration of GAPDH or actin indicated to the right of the WB. For bar graphs
910 in panels (A) and (B), standard error was determined from two replicates. (C) Lysates analyzed in panel
911 (A and B) were also subjected to velocity sedimentation and gradient fractions were analyzed by WB
912 with αGag. The fraction numbers, starting with the first fraction taken from the top of the gradient are
913 indicated above the WB panels. The approximate S-values of the HIV-1 Gag containing complexes are
914 indicated with brackets above the WB panels. The expected migration of p55 Gag is shown to the right
915 of each WB. Quantification of p55 Gag in fractions containing the ~10S, ~80S/150S, and ~500S
916 intermediates shown as the percent of total p55 Gag in the gradient is shown in the bar graphs below the
917 WB panels.
918
919 **Fig 5: Analysis of structure-activity relationships identified an analog that potently inhibits HIV-1**
920 **replication in PBMCs and a site for tags.** (A) Chemical structure of PAV117 analogs is shown with

921 names of positions in the lower benzyl ring corresponding with those in the column headings of the
922 adjacent table. Each compound listed in the adjacent table was tested for inhibition of HIV-1 replication
923 by treatment of MT-2 cells with various doses of compound followed by infection with HIV-1 NL4-3
924 *Renilla* luciferase reporter virus at a MOI 0.02. HIV-1 replication proceeded for 96 hours followed by
925 luciferase activity measurement, which was used to calculate percent inhibition relative to DMSO-
926 treated controls. These data were used to generate dose-response curves and the results are summarized
927 in the adjacent table as the average 50% effective concentration (EC50), the average 50% cytotoxicity
928 concentration (CC50), the selectivity index (SI; ratio of CC50 over EC50). When shown, standard error
929 was determined using the number of replicates indicated after the individual estimate. (B) The blue
930 dose-response curve was generated by treatment of MT-2 cells with various doses of PAV206 followed
931 by infection with HIV-1 NL4-3 *Renilla* luciferase reporter virus at a MOI 0.02. HIV-1 replication was
932 allowed to proceed for 96 hours followed by luciferase activity measurement, which was used to
933 calculate percent inhibition relative to DMSO-treated controls. The EC50 is shown in blue text on the
934 dose-response plot. The CC50, which was determined in parallel using uninfected MT-2 T cells, is
935 marked by vertical dashed line on the dose-response plot and shown in blue text. The orange dose-
936 response curve was generated in a similar manner but using PHA-activated PBMC and an unmodified
937 NL4-3 virus at a MOI of 0.008. After 96 hours, post-infection, media was harvested, and HIV-1
938 infectivity determined on Tzm-bl indicator cells using MUG substrate. These measurements were used
939 to determine percent inhibition relative to DMSO-treated controls. The EC50 is shown in orange text on
940 the dose-response plot. The CC50, which was determined in parallel using uninfected PHA-activated
941 PBMC, is marked by vertical dashed line on the dose-response plot and shown in orange text on the plot.
942 Standard errors determined from three replicates are shown. (C) Dose-response curve generated in the
943 same assay as the blue dose-response curve shown in (B) but using PAV818 instead of PAV206. The
944 EC50 is shown in blue text on the dose-response plot. The CC50, which was determined in parallel

945 using uninfected MT-2 T cells, is marked by vertical dashed line on the dose-response plot and shown in
946 black text.
947
948 **Fig 6: An antiviral analog of PAV-117 colocalizes with HIV-1 Gag in situ.** (A) Shown is a
949 schematic of the proximity ligation assay (PLA). HIV-1 chronically infected 293T cells (293T-HIV) or
950 uninfected 293T cells where treated as indicated beneath the bar graph shown in (B) for approximately
951 sixteen hours. Cells were then fixed and incubated with antibodies (diagramed in black and Y-shaped)
952 to detect biotin-compound (red square), either PAV818 (biotinylated analog of PAV206) or PAV543
953 (biotinylated analog inactive against HIV-1), and Gag (blue) *in situ* followed by incubation with PLA
954 probes (species specific secondary antibodies conjugated to specific oligonucleotides). Sites where
955 biotin-compound and Gag are within 40 nm can undergo the PLA reaction resulting in a strongly
956 florescent spot at those sites (shown as red spots). The PLA assay is followed by concurrent
957 immunofluorescence (IF) against Gag to stain the overall cell. (B) The average number of biotin-Gag
958 PLA spots per cell was determined for each of the tested conditions indicated beneath the bar graph with
959 HIV infected cells, indicated by +, or uninfected cells, indicated by -. Standard error was determined
960 using the number of cells examined (see methods). The * indicates a significant difference between
961 biotin-Gag PLA spots per cell between PAV818 10 μM and PAV543 10 μM treatment ($p < 0.001$). (C)
962 A representative field for each of the treatments quantified in (B) is shown except for DMSO. The
963 treatment is indicated to the left of each set of images. The left-hand image is the biotin-Gag PLA
964 channel shown in grayscale to emphasize the PLA spots, where each spot represents a site where biotin-
965 compound and Gag are within 40 nM. The right-hand image is a merge of the biotin-Gag PLA channel
966 (red), Gag IF channel (green), and DAPI stained nuclei channel (blue). Scalebars, 10 μm.
967
968 **Fig 7: Resistance mutations in Gag or Pol were not observed upon selection in cell culture.** (A) A
969 NL4-3 virus stock was passaged weekly over 37 weeks in the presence of either PAV206 or Nelfinavir

970 starting at 1 x EC50. The concentration of compound was increased 2-fold when infected and
971 compound treated cultures reached maximum viral cytopathic effect (CPE) in a timeframe similar to a
972 DMSO control. Graph plots the fold EC50 concentration vs. week of selection (passage) to illustrate
973 how the selection changed over time for PAV206 (left) or Nelfinavir (right). Red arrows indicate
974 passages that were subjected to sequencing and the approximate region of the genome that was
975 sequenced. (B) For each selection, PAV206 or Nelfinavir, there is a genome map of HIV-1 showing
976 positions of viral open reading frames (ORFs), 5' LTR, and 3' LTR against a number line indicating
977 approximate nucleotide position within the HIV-1 genome. In each case, ORFs where dominant non-
978 synonymous mutations emerged during selection with their respective compound are color coded as
979 follows: Gag in blue, protease in red, env in brown. Beneath the HIV-1 genome maps, dominant non-
980 synonymous mutations identified through sequencing of passages indicated with red arrows in panel (A)
981 from either PAV206 (left) or Nelfinavir (right), are placed according to their position in the genome map
982 shown at the top of panel (B). The passage where mutations were identified is indicated to the left of
983 each genome map line. The mutations are color coded according to the ORF in which they were found,
984 described above. Some mutations have been previously identified as solely culture adaptations and are
985 marked with a double dagger. The Nelfinavir specific mutations are marked with an asterisks.
986
987 **Fig 8: An antiviral PAV-117 analog colocalizes in situ with ABCE1, a host component of assembly**
988 **intermediates.** (A) Shown is a schematic of the proximity ligation assay (PLA). HIV-1 chronically
989 infected 293T cells (293T-HIV) or uninfected 293T cells where treated as indicated beneath the bar
990 graph shown in (B) for approximately sixteen hours. Cells were then fixed and incubated with
991 antibodies (diagramed in black and Y-shaped) to detect biotin-compound (red square), either PAV818
992 (biotinylated analog of PAV206) or PAV543 (biotinylated analog inactive against HIV-1), and ABCE1
993 (orange) *in situ* followed by incubation with PLA probes (species specific secondary antibodies
994 conjugated to specific oligonucleotides). Sites where biotin-compound and ABCE1 are within 40 nm

995 can undergo the PLA reaction resulting in a strongly florescent spot at those sites (shown as red spots).
996 The PLA assay is followed by concurrent immunofluorescence (IF) against ABCE1 to stain the overall
997 cell. (B) The average number of biotin-ABCE1 PLA spots per cell was determined for each of the
998 tested conditions indicated beneath the bar graph with HIV infected cells, indicated by +, or uninfected
999 cells, indicated by -. Standard error was determined using the number of cells examined (see methods).
1000 The * indicates a significant difference in biotin-ABCE1 PLA spots per cell between PAV818 10 μM
1001 and PAV543 10 μM treatment ($p < 0.001$). (C) A representative field for each of the treatments
1002 quantified in (B) is shown except for DMSO. The treatment is indicated to the left of each set of
1003 images. The left-hand image is the biotin-ABCE1 PLA channel shown in grayscale to emphasize the
1004 PLA spots, where each spot represents a site where biotin-compound and ABCE1 are within 40 nM.
1005 The right-hand image is a merge of the biotin-ABCE1 PLA channel (red), Gag IF channel (green), and
1006 DAPI stained nuclei channel (blue). Scalebars, 10 μm.
1007
1008 **Fig 9. An antiviral PAV-117 analog colocalizes *in situ* with DDX6, an RNA granule protein in**
1009 **assembly intermediates.** (A) Shown is a schematic of the proximity ligation assay (PLA). HIV-1
1010 chronically infected 293T cells (293T-HIV) where treated as indicated beneath the bar graph shown in
1011 (B) for approximately sixteen hours. Cells were then fixed and incubated with antibodies (diagramed in
1012 black and Y-shaped) to detect biotin-compound (red square), PAV818 (biotinylated analog of PAV206;
1013 red square), and DDX6 (green diamond) *in situ* followed by incubation with PLA probes (species
1014 specific secondary antibodies conjugated to specific oligonucleotides). Sites where biotin-compound
1015 and DDX6 are within 40 nm can undergo the PLA reaction resulting in a strongly florescent spot at
1016 those sites (shown as red spots). The PLA assay is followed by concurrent immunofluorescence (IF)
1017 against DDX6 to stain the overall cell. (B) The average number of biotin-DDX6 PLA spots per cell was
1018 determined for each of the tested conditions indicated beneath the bar graph. Error bars show SEM
1019 determined using the number of cells examined (see methods). The * indicates a significant difference

1020 in the number of biotin-DDX6 PLA spots between PAV818 10 μM and DMSO treatment ($p < 0.01$). (C)
1021 A representative field for each of the treatment quantified in (B) is shown. The treatment is indicated to
1022 the left of each set of images. The left-hand image is the biotin-DDX6 PLA channel shown in grayscale
1023 to emphasize the PLA spots, where each spot represents a site where biotin-compound and DDX6 are
1024 within 40 nM. The right-hand image is a merge of the biotin-DDX6 PLA channel (red), DDX6 IF
1025 channel (green), and DAPI stained nuclei channel (blue). Scalebars, 10 μm.
1026
1027 **Fig 10: A model for the action of PAV-117, a possible first-in-class selective inhibitor of HIV-1**
1028 **assembly.** Upper diagram shows the model of the host-catalyzed assembly pathway, without inhibition,
1029 that starts with synthesis of HIV-1 Gag to form the early ~10S assembly intermediate. Newly
1030 synthesized ~10S HIV-1 Gag co-opts a preexisting RNA granule to form the ~80S cytosolic
1031 intermediate. In this intermediate HIV-1 Gag is found associated with ABCE1, DDX6, HIV-1 gRNA,
1032 and other host factors. The cytosolic ~80S assembly intermediate targets to host plasma membrane
1033 where continued Gag multimerization leads to the formation of the ~500S assembly intermediate.
1034 Finally, continued HIV-1 Gag multimerization followed by budding results in release of the completed
1035 immature capsid. The lower diagram shows one model for PAV117 activity based on the findings in
1036 this study. Based on our PLA colocalization studies we hypothesis that PAV117 is associated with the
1037 HIV-1 assembly intermediates. Furthermore, it is possible that PAV117 is also associated with the
1038 RNA-granule that is coopted by ~10S Gag, since we find PAV117 colocalized with ABCE1 in the
1039 absence of Gag. Lastly, since we observed a reduction of ~500S assembly intermediate and virus
1040 production in PAV117 treated infected cells, PAV117 may act by blocking progression past the
1041 ~80S/150S assembly intermediate. It is also possible that PAV117 acts early to inhibit progression past
1042 the ~80S cytosolic assembly intermediate.
1043

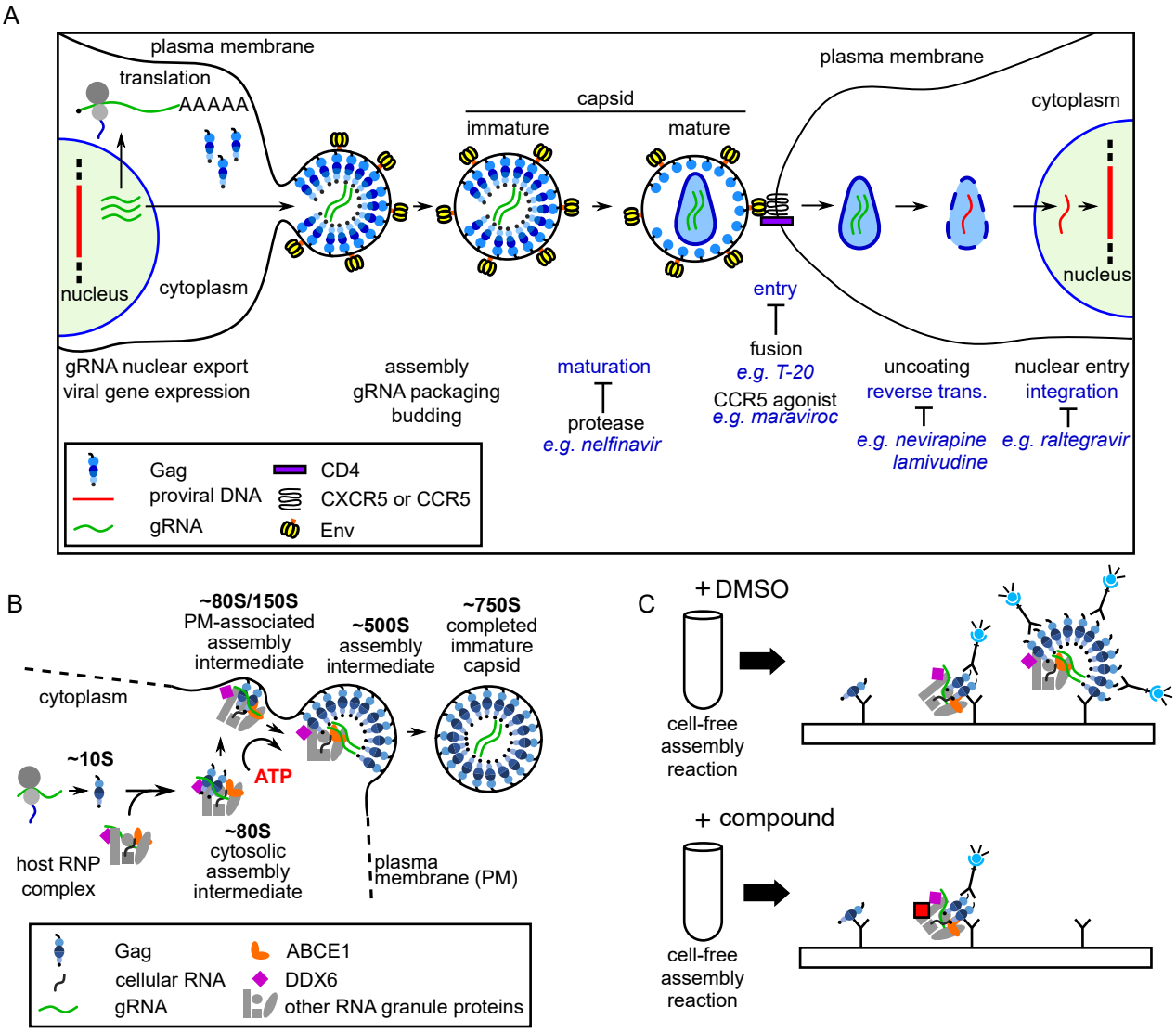

Fig 1: The HIV-1 assembly pathway and HIV-1 assembly drug screen

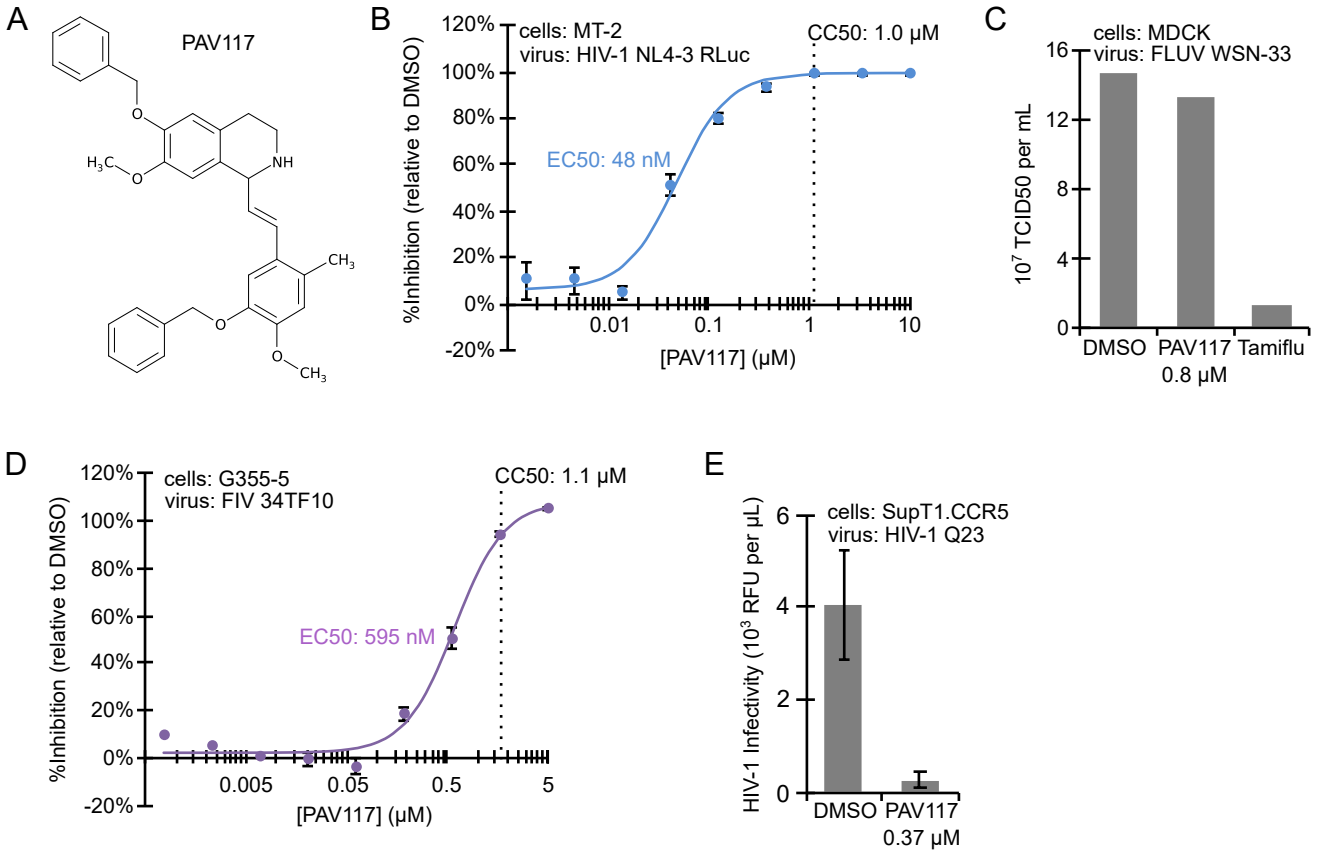

Fig. 2 PAV-117, identified in a cell-extract-based assembly screen, inhibits replication of HIV-1, but not FLUV and FIV, in cell culture.

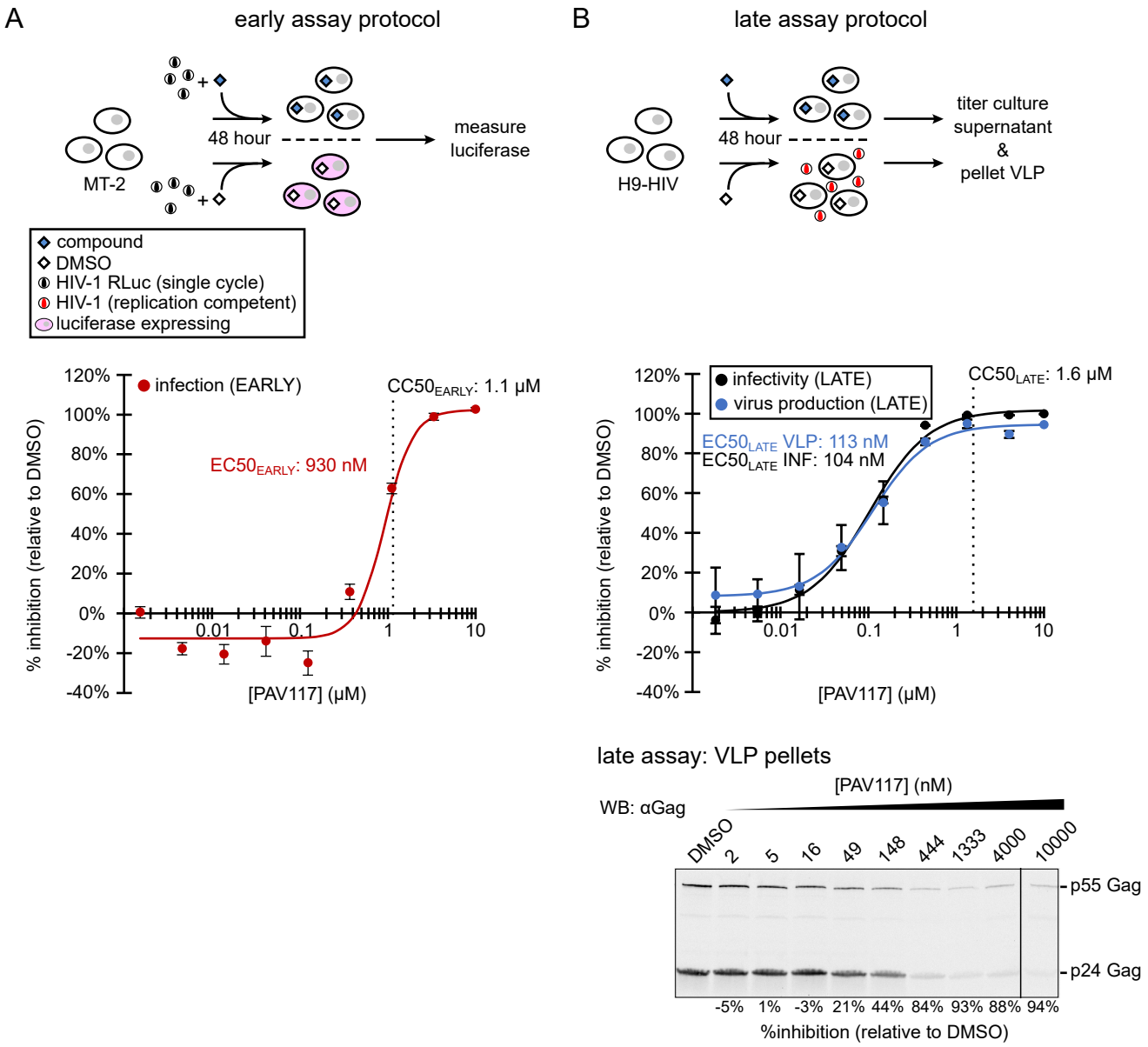

Fig 3: PAV-117 acts late in the HIV-1 life cycle, inhibiting virus production but not specific infectivity.

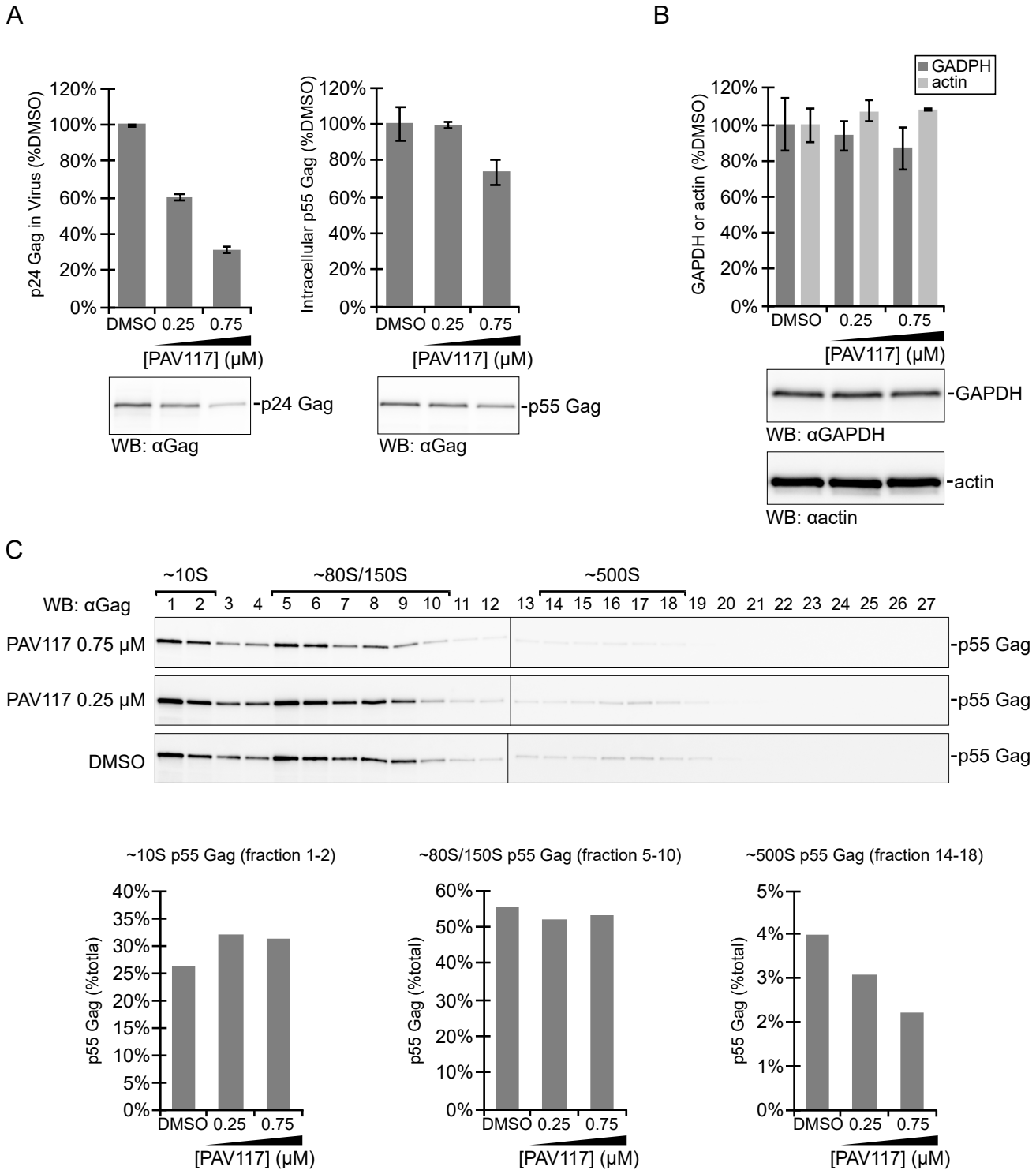

Fig 4: PAV-117 acts during the HIV-1 assembly pathway, after formation of the ~80S intermediate.

A

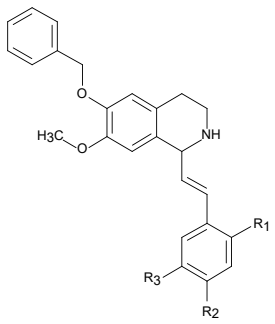

	R_1	R_2	R_3	CC50 (μM)	EC50 (nM)	SI
PAV117	CH_3	O CH_3	O	1.4 ×/÷ 1.5 (n = 6)	102 ×/÷ 2.1 (n = 5)	14
PAV218	CH_3	O CH_3	H	9.7 ×/÷ 1.2 (n = 2)	148 ×/÷ 1.1 (n = 3)	66
PAV220	H	O CH_3	O	3.8 (n = 1)	163 (n = 1)	23
PAV494	H	H	O	4.1 (n = 1)	244 (n = 1)	17
PAV493	H	O CH_3	H	21.0 (n = 1)	565 ×/÷ 1.3 (n = 2)	37
PAV245	CH_3	H	H	3.6 (n = 1)	755 (n = 1)	4.8
PAV492	H	H	H	> 10 (n = 1)	1540 (n = 1)	> 6
PAV206	CH_3	O CH_3	O CH_3	2.2 ×/÷ 1.4 (n = 4)	36 ×/÷ 1.1 (n = 3)	61

B

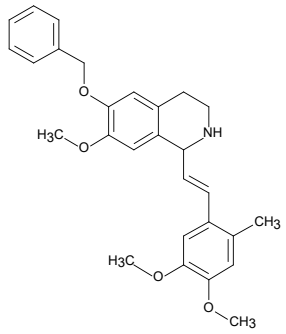

PAV206

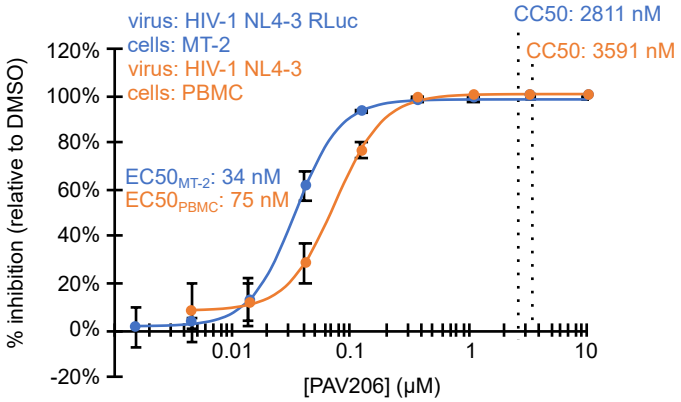

C

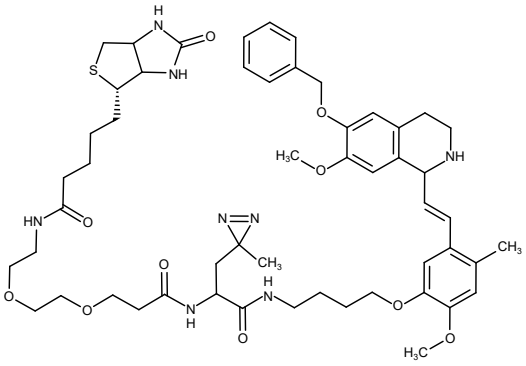

PAV818

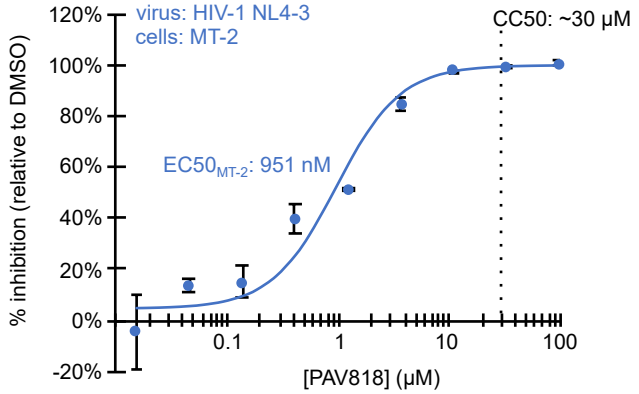

Fig 5: Analysis of structure-activity relationships identified an analog that potently inhibits HIV-1 replication in PBMCs and a site for tags.

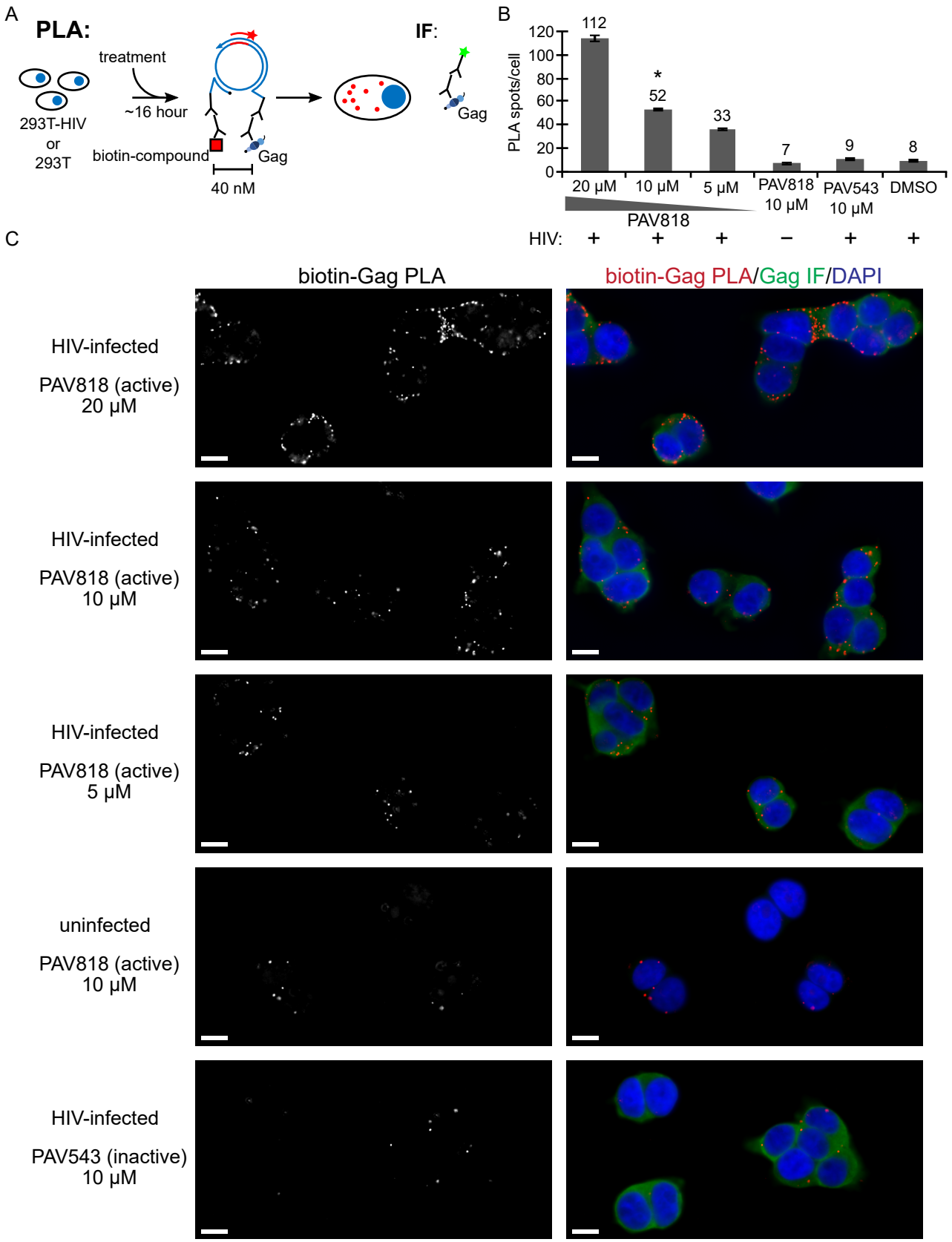

FIG. 6: An antiviral analog of PAV-117 colocalizes with HIV-1 Gag *in situ*.

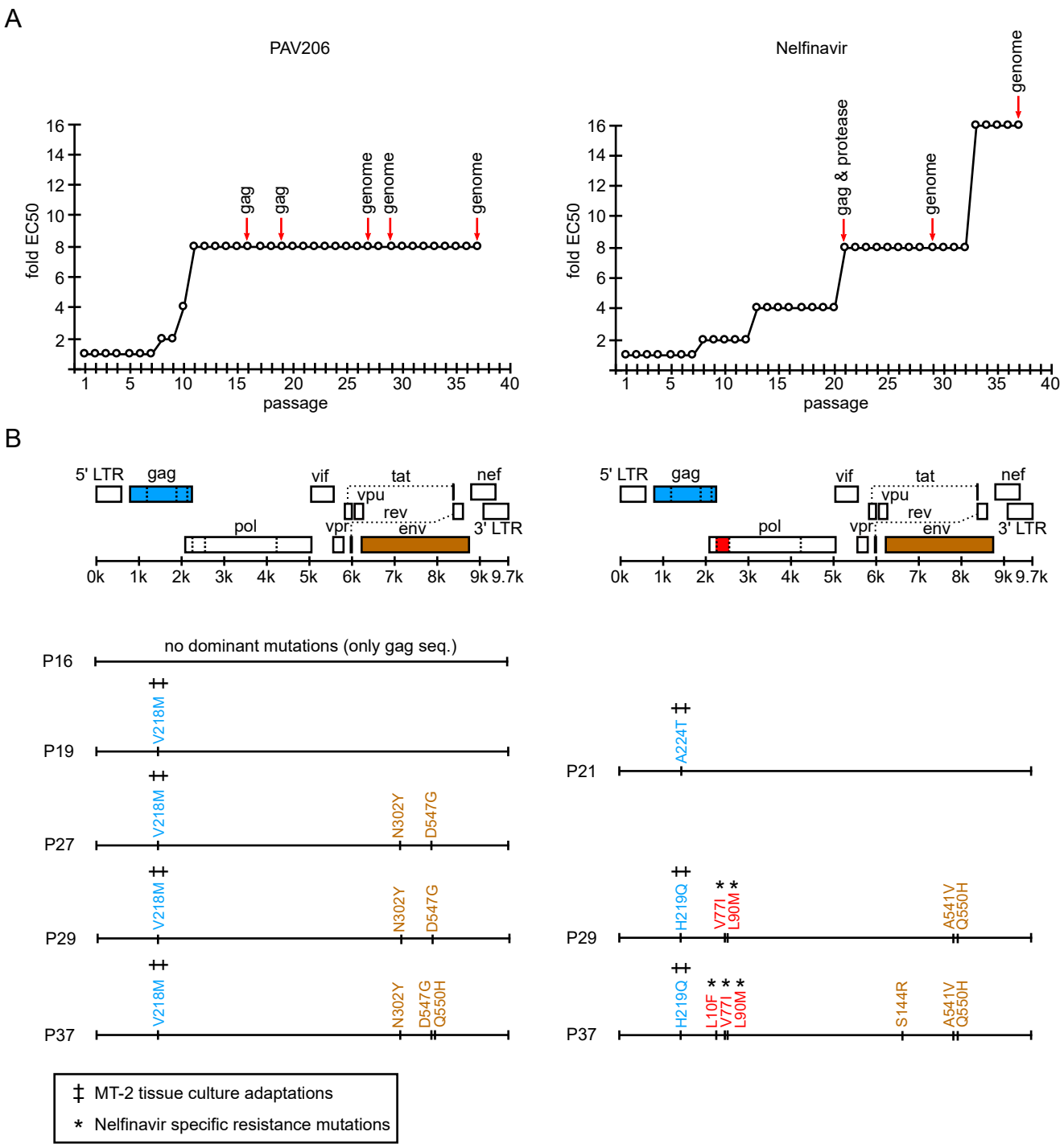

Fig. 7: Resistance mutations in Gag or Pol were not observed upon selection in cell culture

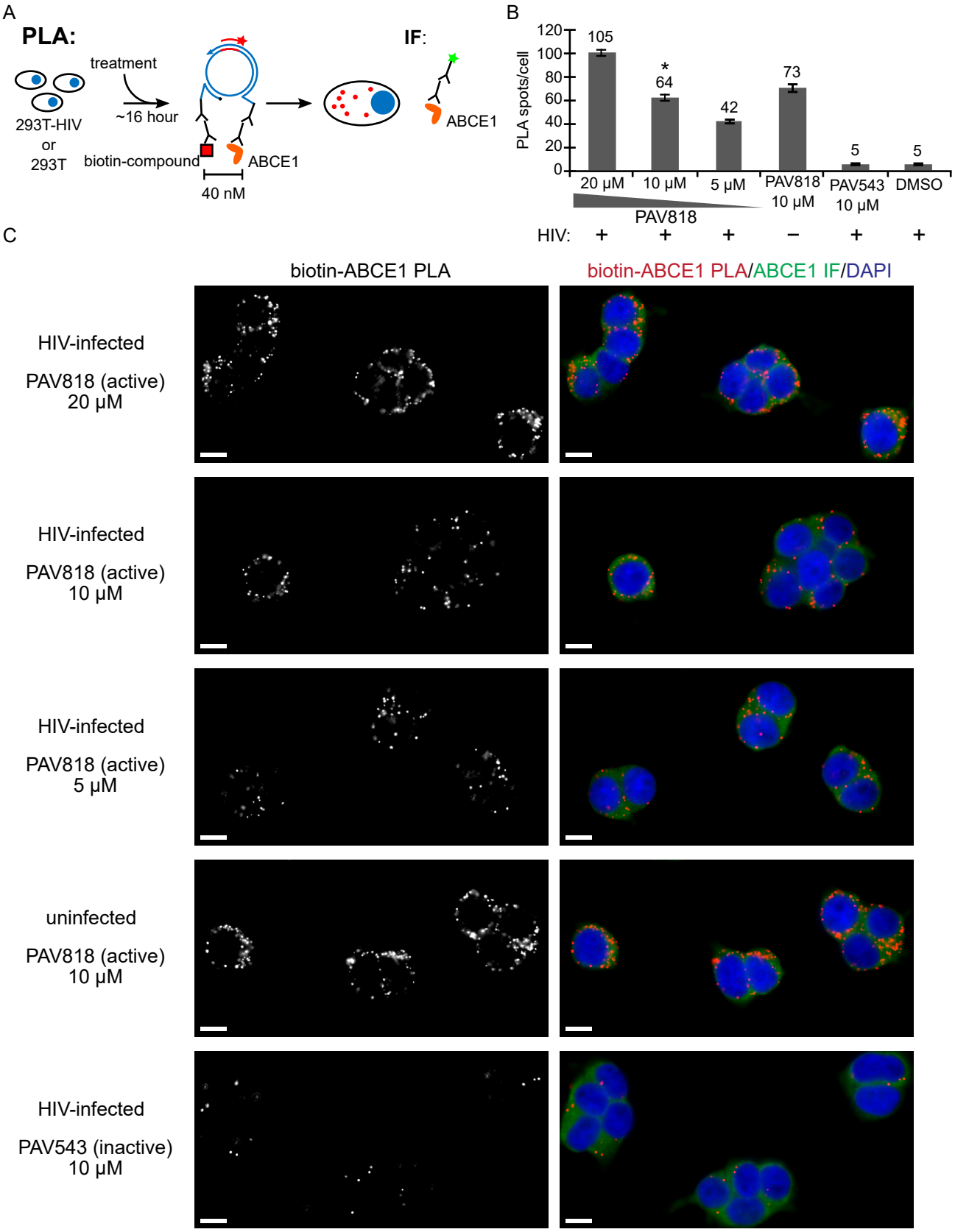

Fig 8: An antiviral PAV-117 analog colocalizes *in situ* with ABCE1, a host component of assembly intermediates.

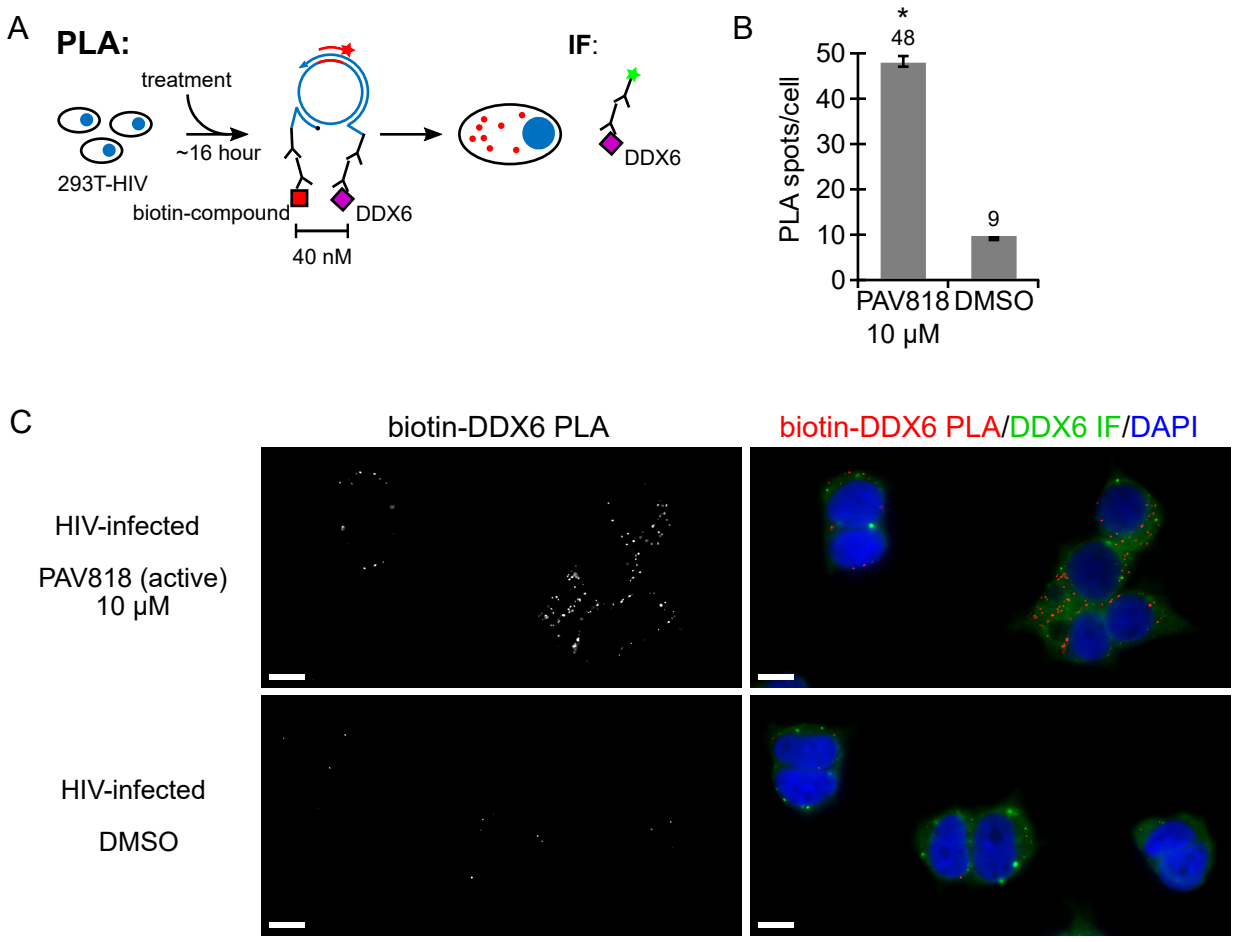

Fig 9. An antiviral PAV-117 analog colocalizes *in situ* with DDX6, an RNA granule protein in assembly intermediates.

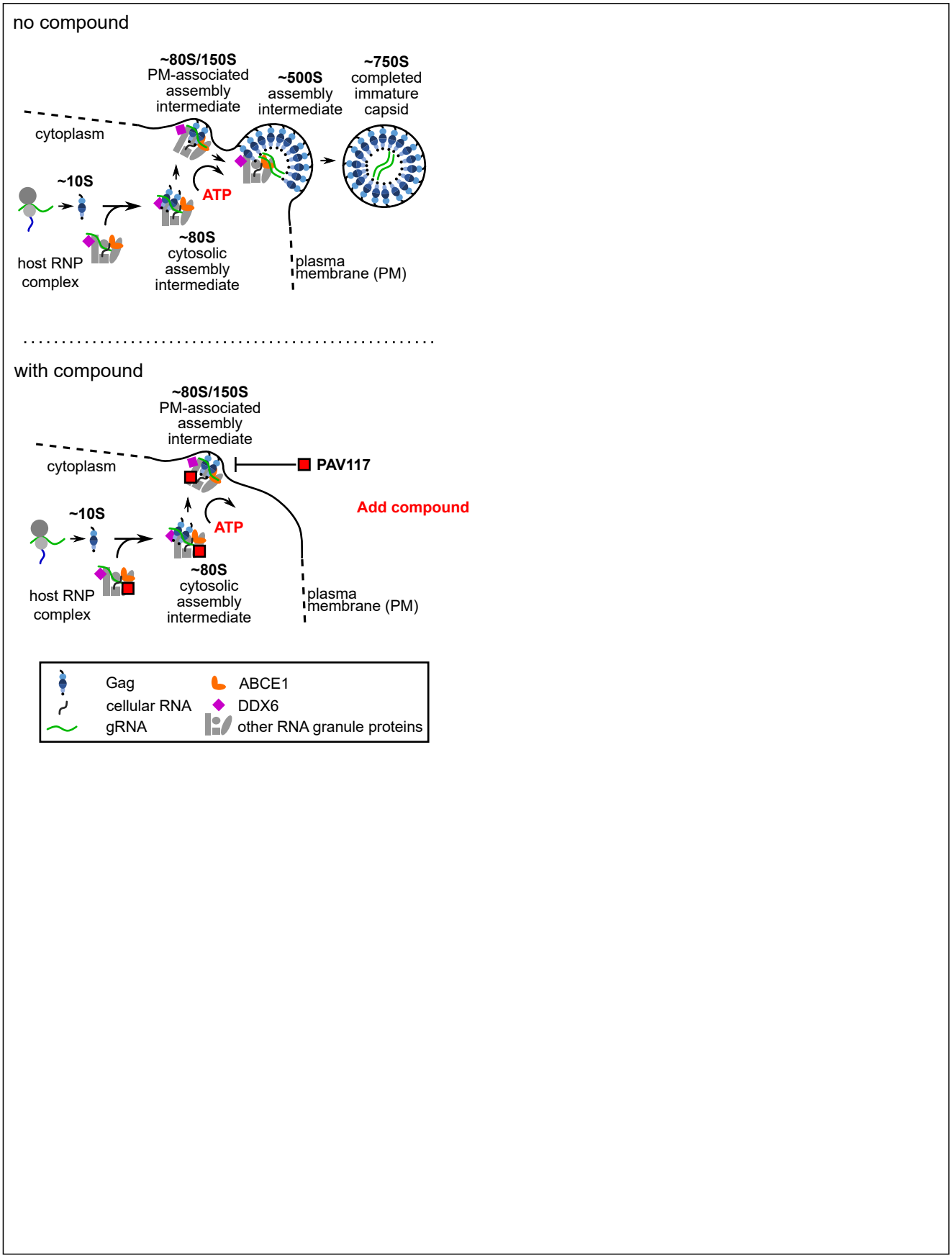

FIG 10: A model for the action of PAV-117, a possible first-in-class selective inhibitor of HIV-1 assembly.

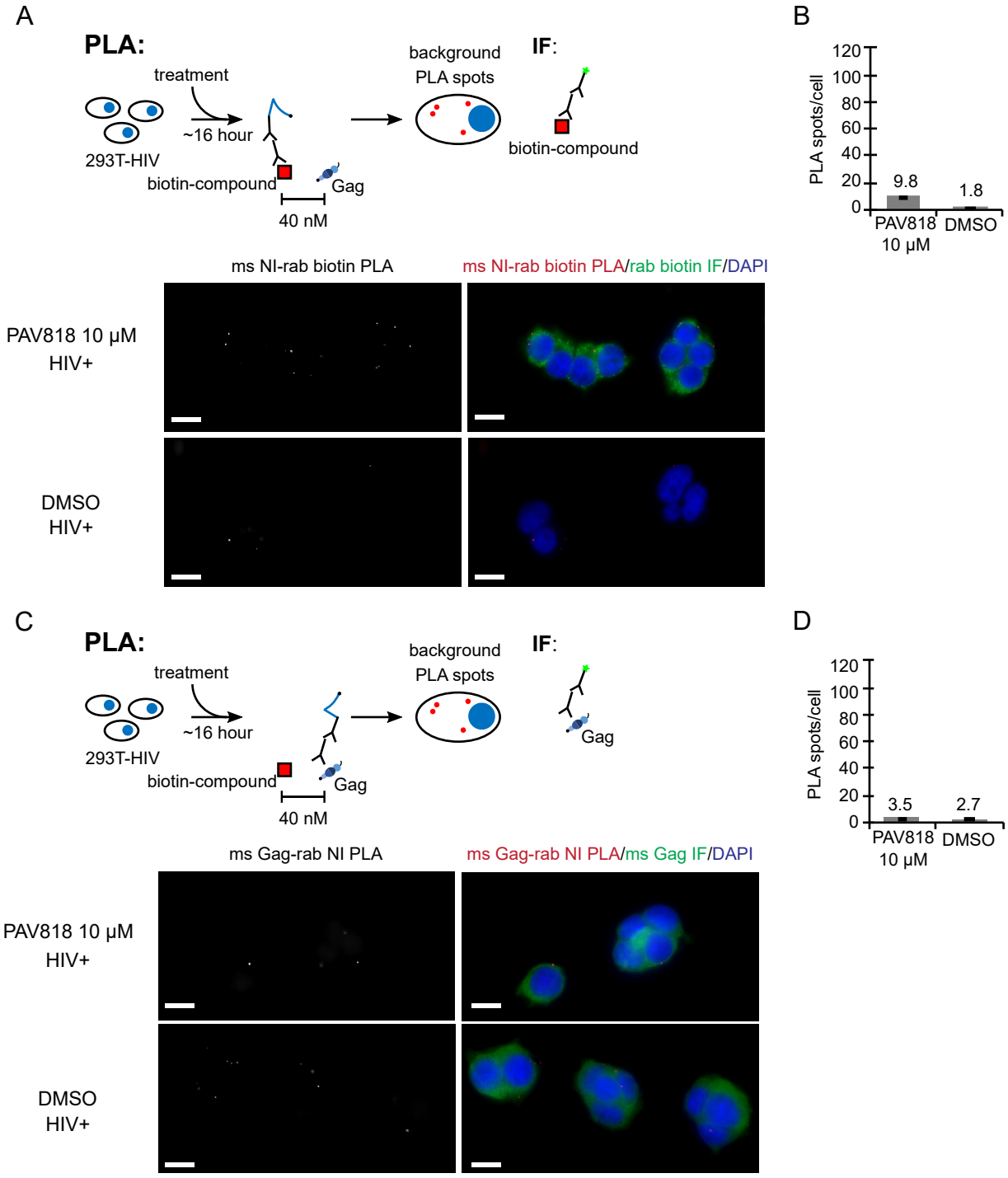

Supplementary Fig 1: Non-immune controls for the biotin-Gag proximity ligation assay

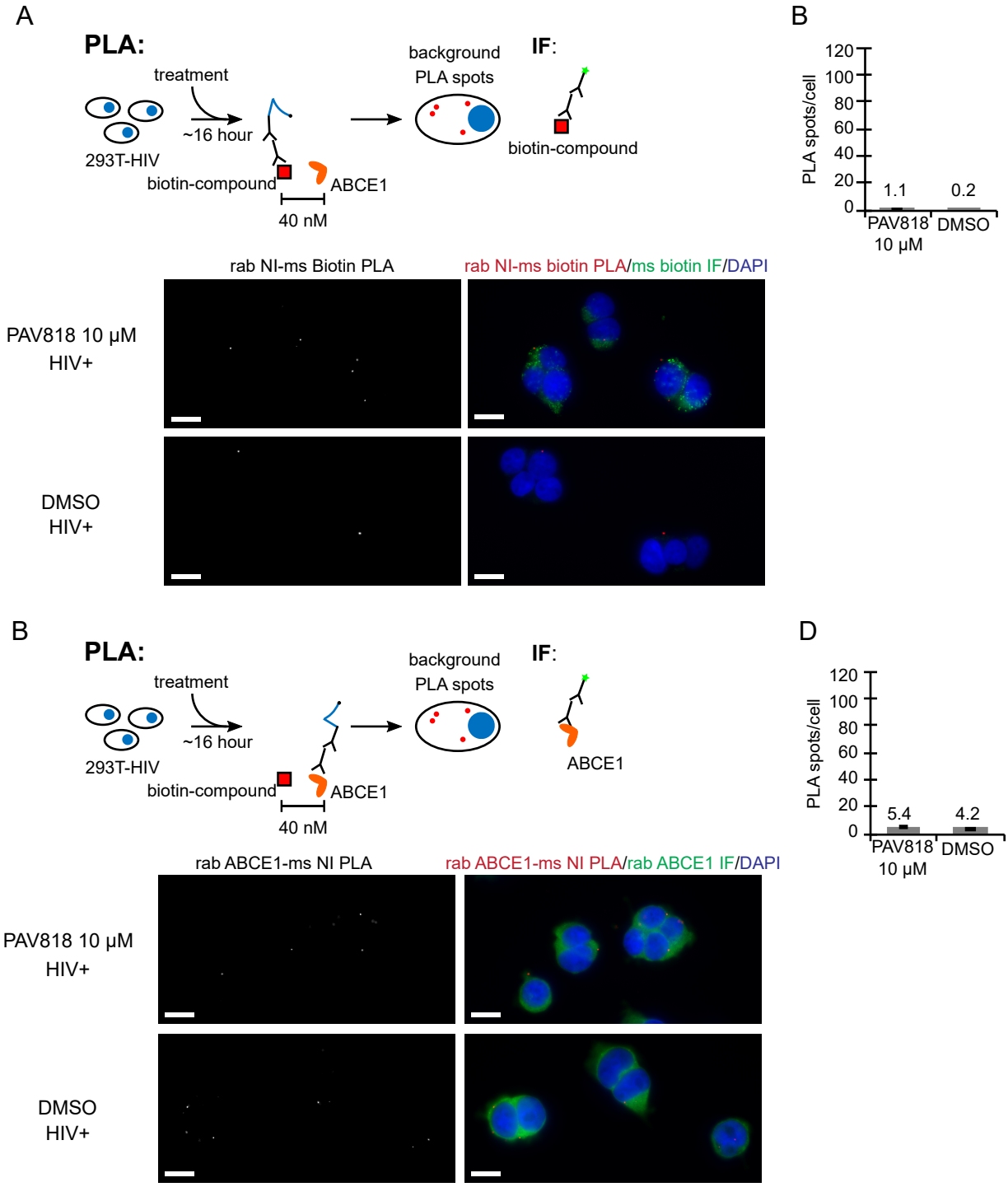

Supplementary Fig 2: Non-immune controls for the biotin-ABCE1 proximity ligation assay